

Article

Origin of Ru-Os Sulfides from the Verkh-Neivinsk Ophiolite Massif (Middle Urals, Russia): Compositional and S-Os Isotope Evidence

Kreshimir N. Malitch ^{1,*}, Inna Yu. Badanina ¹, Elena A. Belousova ², Valery V. Murzin ¹
and Tatiana A. Velivetskaya ³

- ¹ Zavaritsky Institute of Geology and Geochemistry, Ural Branch of the Russian Academy of Sciences, Vonsovsky 15, 620016 Ekaterinburg, Russia; innabadanina@yandex.ru (I.Y.B.); murzin@igg.uran.ru (V.V.M.)
- ² Centre of Excellence for Core to Crust Fluid Systems, Department of Earth and Environmental Sciences, Macquarie University, Sydney, NSW 2109, Australia; elena.belousova@mq.edu.au
- ³ Far East Geological Institute, Far Eastern Branch of the Russian Academy of Sciences, Prospect 100-letya Vladivostoku 159, 690022 Vladivostok, Russia; velivetskaya@mail.ru
- * Correspondence: dunite@yandex.ru

Abstract: This study presents new compositional and S-Os isotope data for primary Ru-Os sulfides within a platinum-group mineral (PGM) assemblage from placer deposits associated with the Verkh-Neivinsk massif, which is part of the mantle ophiolite association of Middle Urals (Russia). The primary nature of Ru-Os sulfides represented by laurite (RuS₂)–erlichmanite (OsS₂) series is supported by occurrence of euhedral inclusions of high-Mg olivine (Fo_{92–94}) that fall within the compositional range of mantle (primitive) olivine (Fo_{88–93}). The sulfur isotope signatures of Ru-Os sulfides reveal a range of δ³⁴S values from 0.3 to 3.3‰, with a mean of 2.05‰ and a standard deviation of 0.86‰ (*n* = 18), implying that the sulfur derived from a subchondritic source. A range of sub-chondritic initial ¹⁸⁷Os/¹⁸⁸Os values defined for Ru-Os sulfides (0.1173–0.1278) are clearly indicative of derivation from a sub-chondritic source. Re-depletion (T_{RD}) ages of the Verkh-Neivinsk Ru-Os sulfides are consistent with prolonged melt-extraction processes and likely multi-stage evolution of highly siderophile elements (HSE) within the upper mantle. A single radiogenic ¹⁸⁷Os/¹⁸⁸Os value of 0.13459 ± 0.00002 determined in the erlichmanite is indicative of a supra-chondritic source of HSE. This feature can be interpreted as evidence of a radiogenic crustal component associated with a subduction event or as an indication of an enriched mantle source. The mineralogical and Os-isotope data point to a high-temperature origin of the studied PGM and two contrasting sources for HSE in Ru-Os sulfides of the Verkh-Neivinsk massif.

Keywords: Ru-Os sulfides; laurite; erlichmanite; sulfur isotopes; osmium isotopes; ophiolite; mantle; Verkh-Neivinsk massif; Urals; Russia



Citation: Malitch, K.N.; Badanina, I.Y.; Belousova, E.A.; Murzin, V.V.; Velivetskaya, T.A. Origin of Ru-Os Sulfides from the Verkh-Neivinsk Ophiolite Massif (Middle Urals, Russia): Compositional and S-Os Isotope Evidence. *Minerals* **2021**, *11*, 329. <https://doi.org/10.3390/min11030329>

Academic Editors: Shoji Arai and Mauricio Calderón

Received: 31 December 2020

Accepted: 17 March 2021

Published: 22 March 2021

Publisher's Note: MDPI stays neutral with regard to jurisdictional claims in published maps and institutional affiliations.



Copyright: © 2021 by the authors. Licensee MDPI, Basel, Switzerland. This article is an open access article distributed under the terms and conditions of the Creative Commons Attribution (CC BY) license (<https://creativecommons.org/licenses/by/4.0/>).

1. Introduction

Dominance of Ru-Os-Ir minerals over other platinum-group minerals (PGM) is considered a typical feature of podiform chromitites within the residual mantle in ophiolite-type dunite-harzburgite massifs worldwide [1–15], among others. According to equilibrium phase diagrams, experimental results, and empirical data, Ru-Os–Ir alloys and Ru-Os sulfides are considered to be formed during the very early stages of magmatic differentiation, under low fugacity of sulfur, and high-temperature conditions [11,16–23]. Ru-Os sulfides from podiform chromitites within the oceanic mantle are particularly important because they are believed to preserve the isotopic values of the sources of highly siderophile elements (HSE) and sulfur from which these Ru-Os sulfides were formed/crystallized. Usefulness of S-isotopic information collected on Ru-Os sulfides derived from the oceanic mantle has been outlined by Hattori et al. [24], whereas Os isotope data gained for Ru-Os-Ir

alloys and sulfides from the dunite-harzburgite massifs worldwide [12,25–36], among others, and Ru-Os-Ir alloys from placer deposits [37–43] shed new insights on the multi-stage evolution history of PGM in mantle-derived ultramafic complexes. Among different points of view on the formation of chromitites and PGM, a significant place is given to the osmium isotope data of PGM, which are discussed in the framework of (i) the long-term evolution of the upper mantle, (ii) the heterogeneity of mantle derivatives, and (iii) the interaction of various sources of PGE/HSE [12,44].

The Urals is a unique structure of the Earth, where the main types of ultramafic massifs formed in various geodynamic settings (continental, oceanic, and island-arc) are found. More than a century of studies of the oceanic dunite-harzburgite massifs of the Urals have shown that both the rocks and the associated types of chromite and PGM were formed in a wide time interval, experienced complex processes of high-temperature plastic deformations, along with dynamic recrystallization; at the same time, they also experienced destruction and amalgamation of individual blocks into larger massifs (complexes).

The Verkh-Nevinsk massif, a typical representative of the mantle ophiolitic association at the Middle Urals (Figure 1a), is characterized by primary and secondary PGM assemblages [45]. The primary PGM assemblage, which is dominated by Ru-Os-Ir alloys over Ru-Os sulfides, Pt-Fe alloys, and other PGM, are typical for chromitites, whereas both the primary and secondary PGM assemblages are found in placer deposits of the Vostochny Shishim River draining different lithological units of the Verkh-Neivinsk massif (Figure 2). Secondary PGM assemblages usually form the outer part of polyphase aggregates, which contain a core composed of a Ru-Os-Ir alloy, rimmed by secondary As-bearing laurite, irarsite (IrAsS), and tolovkite (IrSbS).

Particularities of their chemistry and the physicochemical conditions of formation of Ru-Os-Ir alloys are given elsewhere [22,46–48]. The previously collected Os-isotope data for primary Ru-Os-Ir alloys and Ru-Os sulfides from the Verkh-Nevinsk massif revealed a wide range of sub-chondritic $^{187}\text{Os}/^{188}\text{Os}$ values (from 0.1162 to 0.1346 [49,50]), whereas first S-isotope data for Ru-Os sulfides showed a restricted range of $\delta^{34}\text{S}$ values (from 0.2 to 2.3‰ [51]). Both datasets were interpreted as being consistent with a deep-seated source of highly siderophile elements (HSE) and sulfur.

To gain further insight into the origin of Ru-Os sulfides, we have carried out a combined mineralogical and isotope study of laurite (RuS_2)–erlichmanite (OsS_2) series within a primary PGM assemblage from placer deposit linked to the Verkh-Neivinsk massif. Here, we consider new S-isotope data for 18 Ru-Os sulfide grains, for which Os-isotope data were previously collected on the same spots within PGM samples (16 samples from Reference [50], and 2 new samples). These data are compared with S-isotope data for Ru-Os sulfides [24,51] and Os-isotope data for ultramafic rocks, Ru-Os sulfides and Ru-Os-Ir alloys [49,50,52–67]. Information on genetic features of PGM formation is supplemented by compositional data of solid inclusions typical of the studied Ru-Os sulfides. We integrate an application of electron microprobe analyses of Ru-Os sulfides and solid inclusions within PGM, Re-Os LA-MC-ICP-MS analyses of Ru-Os sulfides and coexistent Os-rich alloys, and S-isotope LA-ICP-MS analyses of Ru-Os sulfides, aiming at (i) evaluating compositional signatures of different morphological types of Ru-Os sulfides, and (ii) constraining the sources of HSE and sulfur within this fragment of the Uralian mantle. This study is part of a larger attempt to elucidate the mantle versus crustal origin of HSE/S in oceanic and subcontinental mantle settings [12,22,24–26,34,35,49–67], among others.

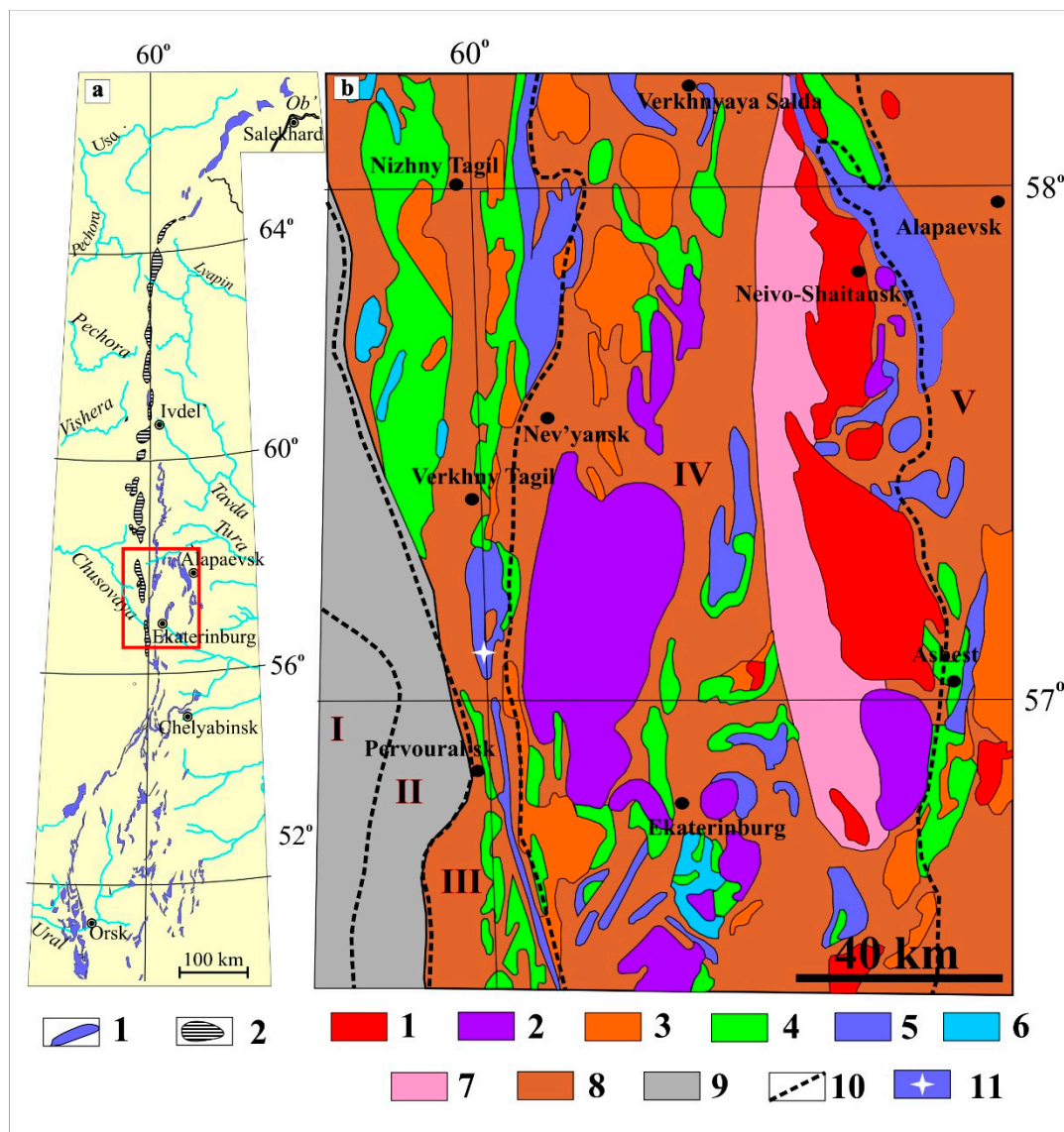


Figure 1. (a) Scheme of location of ophiolite- and zoned-type massifs of the Urals. (1) dunite-harzburgite ophiolite-type massifs, (2) dunite-clinopyroxenite-gabbro zoned-type massifs of the Platinum belt. Box corresponds to inset in Figure 1b. (b) Tectonic scheme of the Middle Urals and position of the Verkh-Neivinsk massif. (1–6) intrusive formations: (1) granitic (granite, granodiorite, alaskite); (2) granitoid (granodiorite, tonalite, granite); (3) plagiogranitic (plagiogranite, quartz diorite); (4) gabbroic (gabbro, gabbro-norite, diorite); (5) dunite-harzburgite (dunite, harzburgite, serpentinite, chromitite); (6) dunite-clinopyroxenite (dunite, chromitite, wehrlite, clinopyroxenite, hornblende); (7) rocks of the amphibolite, amphibolite-gneiss, gneiss, and migmatite associations; (8) volcanogenic sedimentary rocks of the island arc sector of the Urals; (9) flysch, flyschoid, molasse, and terrigenous-carbonate, and carbonate formations of the continental sector of the Urals; (10) boundaries of mega zones ((I) Western Urals, (II) Central Urals, (III) Tagil-Magnitogorsk, (IV) Eastern Urals, (V) Transurals); (11) sampling location.

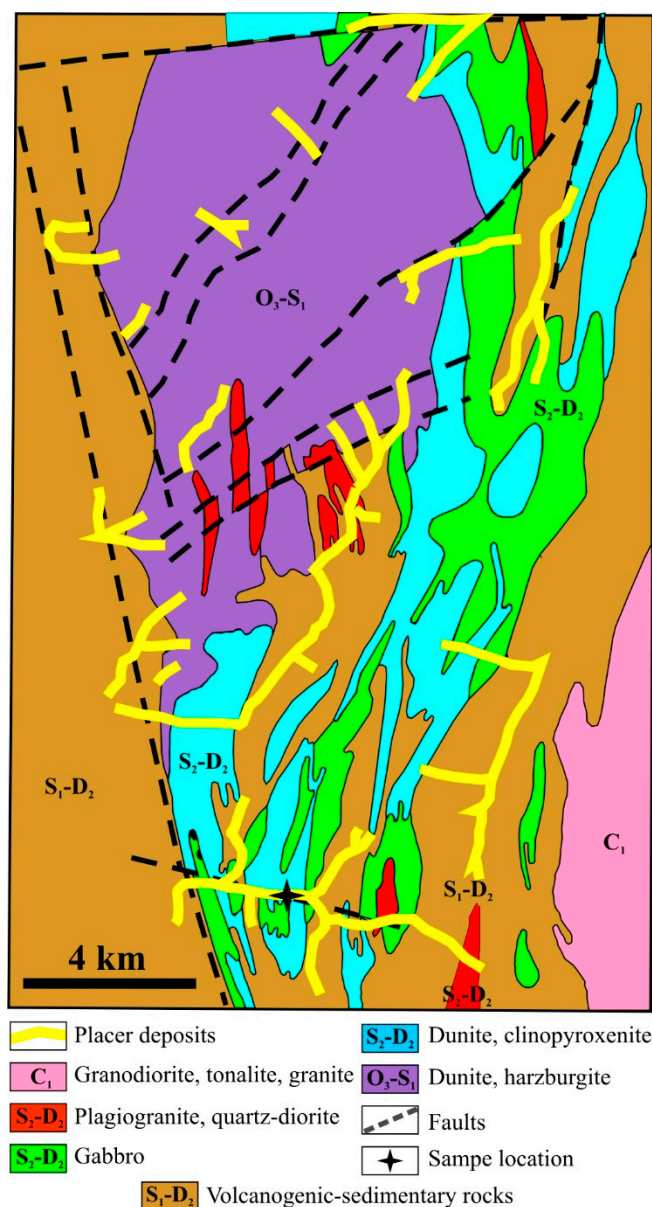


Figure 2. Schematic geological map of the Verkh-Neivinsk massif with locations of Au-PGE placer deposits and studied PGM grains.

2. Geological Characteristics of Samples

The Verkh-Neivinsk massif is situated at the junction of the Tagil Megasyntorium and the East Ural Uplift in the zone of the Serov–Mauk deep-seated fault (Figure 1b). It is composed of two complexes: dunite-harzburgite complex that comprises the inner part of the massif and dunite-clinopyroxenite-gabbro complex developed at the periphery (Figure 2). The former complex is attributed to the Late Ordovician–Early Silurian (O_3-S_1), whereas the latter has Middle Silurian–Middle Devonian (S_2-D_2) age [45]. Sixty-eight occurrences and small deposits of chromite ores were discovered in lithological units of both complexes. The main occurrences of noble metals (native gold and PGM) are related to the placer deposits of modern and ancient river valleys. Representative collection of 685 grains of Ru-Os-Ir minerals in a size range from 0.1 to 3 mm was sampled from a gold production concentrate during prospecting of the Tertiary and Quaternary sediments of the Vostochny Shishim River that are confined to the southern part of the Verkh-Neivinsk massif (Figure 2). According to Badanina et al. [47], PGM grains are mainly represented by sub-euhedral and euhedral crystals with subordinate amount of crystal aggregates, among which Ru-Os-Ir

alloys (83.5%) prevail over Ru-Os sulfides (15.3%) and Pt-Fe alloys (1.2%). In terms of morphology, Ru-Os-Ir alloys are characterized by well-preserved combinations of basal plane, hexagonal prism, and hexagonal dipyramid, whereas Ru-Os sulfides and Pt-Fe alloys have rough, sometimes shallow surfaces of crystal grains and crystal aggregates. Majority of primary PGM are monophasic. The remaining polyminerallic grains are dominated by IPGE alloys (Os, Ir, and Ru), with minor amounts of one or several other PGM inclusions, including laurite RuS₂, kashinite Ir₂S₃, cuprorhodsite CuIr₂S₄, cooperite PtS, Pt-Fe alloys, irarsite IrAsS, hollingworthite RhAsS, keithconnite Pd₂₀Te₇, and ruthenarsenite RuAs [47]. The PGM grains analyzed in this study are nuggets (crystals and aggregates) that fall within a size range between 0.5 and 1.5 mm.

3. Analytical Techniques

Microprobe analyses of Ru-Os sulfides and mineral inclusions were carried out with a CAMECA SX-100 equipped with five WDS spectrometers and a Bruker energy dispersive spectrometer system at Common Use Center “Geoanalyst” of Institute of Geology and Geochemistry, Ural Branch of the Russian Academy of Sciences (Ekaterinburg, Russia). Quantitative WDS analyses were performed at 25 kV accelerating voltage and 20 nA sample current, with a beam diameter of about 1 μm. The following X-ray lines and standards have been used: RuLα, RhLα, PdLβ, OsMα, IrLα, PtLα, NiKα (all native element standards), FeKα, CuKα, SKα (all chalcopyrite), and AsLα (sperrylite). Corrections were performed for the interferences involving Ru-Rh, Ru-Pd, and Ir-Cu. All elements but Os, Ir, Ru, Rh, Fe, and S were found to be below the statistically reliable detection limits under the analytical conditions. Additional details of the analytical procedures used are described in Badanina et al. [47].

Twenty-six in-situ Os-isotope analyses of Ru-Os sulfides and coexistent Ru-Os-Ir alloys were carried out at the Geochemical Analysis Unit at the CCFS/GEMOC laboratories (Macquarie University, Sydney, Australia) using analytical methods reported in other publications [32,34,64,67]. These analyses used a Nu Plasma Multi-collector ICP-MS attached to a New Wave/Merchantek UP 213 laser microprobe. Ablation was carried out with a frequency of 4 Hz, energies of 1–2 mJ/pulse, and a spot size of 15 μm. A standard NiS bead (PGE-A) with 199 ppm Os [68] and ¹⁸⁷Os/¹⁸⁸Os = 0.1064 [67], along with a natural Os alloy (i.e., Os_{1.0}) from the Guli massif [69,70], were analyzed between PGM samples to monitor any drift in the Faraday cups. The overlap of ¹⁸⁷Re on ¹⁸⁷Os was corrected by measuring the ¹⁸⁵Re peak and using ¹⁸⁷Re/¹⁸⁵Re = 1.6742. All the analyzed grains have ¹⁸⁷Re/¹⁸⁸Os lower than 0.005, thus ensuring that the isobaric interference of ¹⁸⁷Re on ¹⁸⁷Os was precisely corrected [31]. The data were collected using the Nu Plasma time-resolved software, which allows the selection of the most stable intervals of the signal for integration. For laurite with grain sizes between 50 and 1000 μm and Os average contents of ~10 at.%, a typical run duration of ~75 s was achieved with an average signal intensity of Os~7.8 V on the Faraday cups. This gives a precision for ¹⁸⁷Os/¹⁸⁸Os ranging from 2.1 × 10⁻⁵ to 9.2 × 10⁻⁵ (SE). The external reproducibility of ¹⁸⁷Os/¹⁸⁸Os for the PGE-A standard during the period of measurements was 0.00013 (2σ SD, n = 15) with a mean value of 0.10652. Repeated analyses of a natural crystal of native osmium, which has been used to check the validity of the LA MC ICP-MS measurements, yield ¹⁸⁷Os/¹⁸⁸Os = 0.12452 ± 0.00004 (2σ SD, n = 27). This perfectly matches two previously measured LA MC ICP-MS analyses (Neptune MC ICP-MS attached to a New Wave Compex-2 DUV 193 laser microprobe, Russian Geological Institute, St. Petersburg, Russia) for the same Os grain with ¹⁸⁷Os/¹⁸⁸Os ranging between 0.124546 ± 0.000007 and 0.124566 ± 0.000013. Rhenium-depletion model ages (T_{RD}) and Re-Os model ages (T_{MA}) were defined previously by other authors [71,72]. Rhenium-depletion model ages (T_{RD}) are calculated using the equation $T_{RD} = (1/\lambda) \times \ln(((^{187}\text{Os}/^{188}\text{Os})_{\text{sample}} - (^{187}\text{Os}/^{188}\text{Os})_{\text{CHUR}}) / ((^{187}\text{Re}/^{188}\text{Os})_{\text{CHUR}} + 1))$, where λ represent a ¹⁸⁷Re decay constant of 1.666 × 10⁻¹¹ a⁻¹ [73], whereas sample and CHUR parameters represent present-day values. The T_{RD} in this study were calculated relative to an Enstatite Chondrite Reservoir (T^{ECR}) with ¹⁸⁷Re/¹⁸⁸Os = 0.421 ± 0.013 [74] and present-day

$^{187}\text{Os}/^{188}\text{Os} = 0.1281 \pm 0.0004$. Alternative $^{187}\text{Os}/^{188}\text{Os}$ values for the present-day mantle, in widespread use for calculation of model ages, are 0.12736 [75], 0.1270 [71], and 0.1296 ± 0.0008 [76], where $^{187}\text{Re}/^{188}\text{Os}$ is taken as 0.40186 [71]. Calculations using the first two $^{187}\text{Os}/^{188}\text{Os}$ estimates would result in model ages that are approximately 0.15–0.2 Ga younger. If the $^{187}\text{Os}/^{188}\text{Os}$ value of primitive upper mantle (PUM) is used, the model ages of PGM are approximately 0.2 Ga older.

Eighteen S-isotope analyses were subsequently performed at the Laboratory of Stable Isotope within Common Use Center of the Far East Geological Institute, Far Eastern Branch of the Russian Academy of Sciences (Vladivostok, Russia). In situ S-isotope data were collected on the same spots within Ru-Os sulfide grains, for which Os-isotopic composition was analyzed previously. Sample preparation for mass spectrometric isotope analysis of sulfur was carried out using a femtosecond laser ablation system, NWR Femto, in combination with a reactor for sulfide aerosol conversion into SF_6 gas, a cryogenic and chromatographic purification system, and an isotope ratio mass spectrometer (FsLA-GC-IRMS) [77,78]. Isotope ratios of sulfur were measured using a MAT-253 mass spectrometer (Thermo Fisher Scientific, Germany) equipped with a Faraday cup for simultaneous measurements of the ion currents at m/z 127 ($^{32}\text{SF}_5^+$) and 129 ($^{34}\text{SF}_5^+$). The measurements were carried out relative to the laboratory working standard, calibrated to the international standards IAEA-S-1, IAEA-S-2, and IAEA-S-3. The sulfur isotope composition in the sample was calculated as $\delta^{34}\text{S} = ((^{34}\text{S}/^{32}\text{S})_{\text{sample}} - (^{34}\text{S}/^{32}\text{S})_{\text{standard}}) / (^{34}\text{S}/^{32}\text{S})_{\text{standard}} \times 10^3$ and expressed in ‰ with respect to reference standard VCDT (Vienna Canyon Diablo Troilite). Average accuracy of $\delta^{34}\text{S}$ analyses was better than 0.2‰ (2σ). Further details of analytical methods are presented elsewhere [77,78].

4. Results

4.1. Compositional Characteristics of Ru-Os Sulfides, Os-Rich Alloys, and High-Magnesian Olivine from Primary PGM Assemblage

Typical morphological features, characteristic textures of Ru-Os sulfides, formed by single relatively large grains and small inclusions in Os-Ir alloy grains (termed as type 1 and 2, respectively), and associated minerals are illustrated in Figures 3–5. Representative results of 48 electron microprobe WDS analyses of Ru-Os sulfides and associated Os-rich alloys (out of a total of 219 analyses) and 9 electron microprobe WDS analyses of high-Mg olivine inclusions are shown in Tables 1–3 and Figure 6.

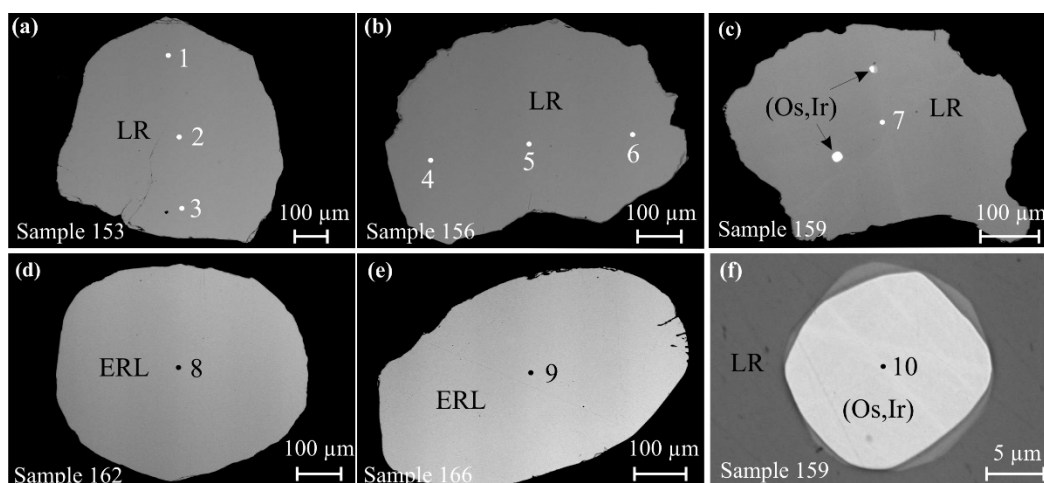


Figure 3. Back-scattered images of laurite grains of type 1 at Verkh-Neivinsk: (a)—sample 153, (b)—sample 156, (c)—sample 159, (d)—sample 162, (e)—sample 166, (f)—detail of Figure 2c. LR—laurite, ERL—erlichmanite, (Os,Ir)—iridian osmium. Numbers 1–10 denote areas of electron microprobe analyses corresponding to the same numbers in Tables 1 and 2.

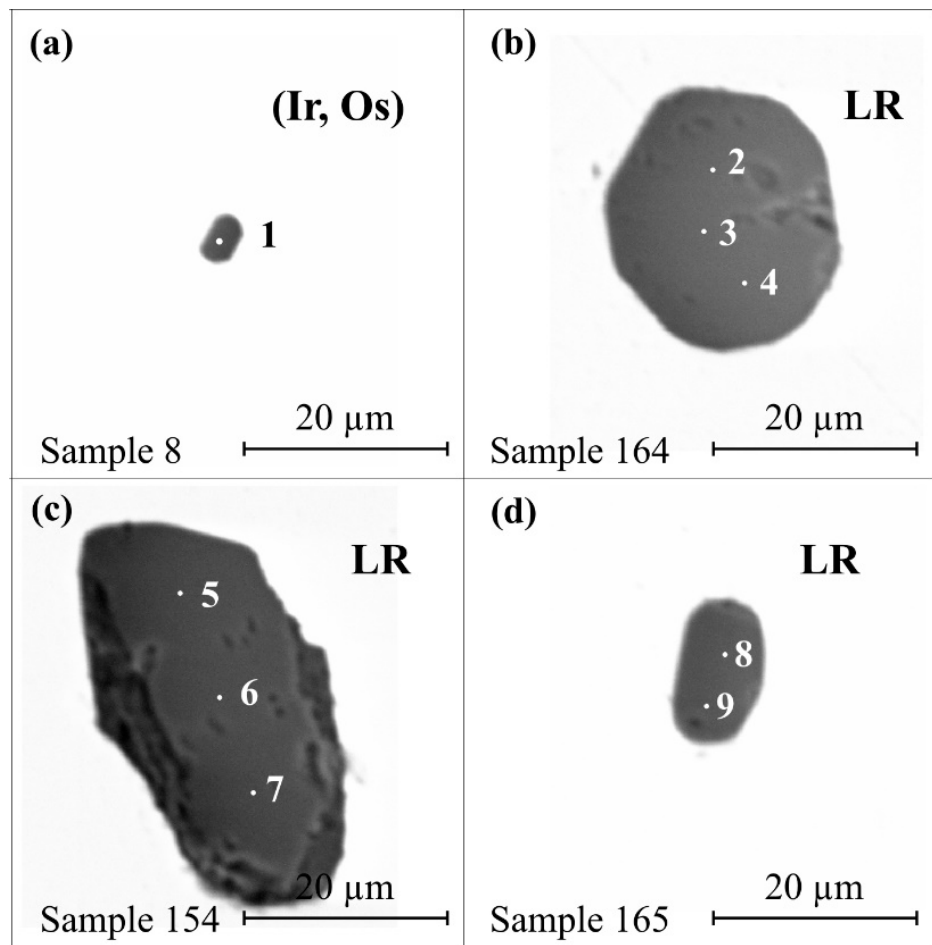


Figure 4. Back-scattered electron images of forsterite inclusions in: (a) osmium iridium (Os,Ir), (b–d) laurite (LR). Numbers 1–9 denote areas of electron microprobe analyses corresponding to the same numbers in Table 3.

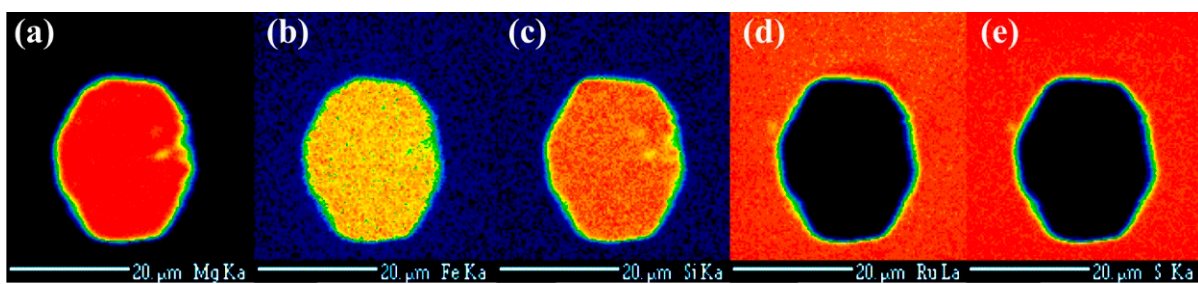


Figure 5. X-ray maps of high-Mg olivine inclusion in laurite (sample 164). (a)—MgK α , (b)—FeK α , (c)—SiK α , (d)—RuL α , (e)—SK α .

Table 1. Electron microprobe analyses of Ru-Os sulfides of type 1 from the Verkh-Neivinsk massif.

Analysis	1	2	3	4	5	6	7	8	9
Sample #	153	153	153	156	156	156	159	162	166
Mineral	LR	ERL	ERL						
Figure	Figure 3a	Figure 3a	Figure 3a	Figure 3b	Figure 3b	Figure 3b	Figure 3c	Figure 3d	Figure 3e
	wt. %								
Fe	b.d.l.	b.d.l.	0.17	0.38	0.40	0.32	b.d.l.	b.d.l.	b.d.l.
Ni	b.d.l.	b.d.l.	b.d.l.	0.23	b.d.l.	b.d.l.	b.d.l.	b.d.l.	b.d.l.
Ru	37.24	36.52	37.10	39.20	38.08	38.89	31.69	12.74	21.48
Rh	0.27	0.39	0.27	0.26	0.25	0.29	0.04	0.11	0.01
Os	19.16	19.08	19.58	20.79	21.34	21.53	33.04	51.23	42.41
Ir	10.38	10.71	9.48	5.96	6.10	5.52	3.32	7.81	5.88
S	33.24	33.08	33.81	33.87	33.80	33.42	32.13	28.17	29.63
As	b.d.l.								
Total	100.29	99.78	100.41	100.69	99.97	99.97	100.22	100.06	99.40
	at. %								
Fe	0.00	0.00	0.19	0.43	0.45	0.36	0.00	0.00	0.00
Ni	0.00	0.00	0.00	0.00	0.25	0.00	0.00	0.00	0.00
Ru	23.57	23.27	23.24	24.27	23.78	24.39	20.80	9.58	15.29
Rh	0.17	0.25	0.16	0.16	0.15	0.18	0.03	0.08	0.01
Os	6.45	6.46	6.52	6.84	7.08	7.18	11.53	20.47	16.04
Ir	3.46	3.59	3.12	1.94	2.00	1.82	1.15	3.09	2.21
S	66.35	66.44	66.77	66.11	66.54	66.07	66.49	66.78	66.46
Ru #	78	78	78	78	77	77	64	32	49

LR—laurite, ERL—erlichmanite, Ru# = $100 \times \text{Ru at. \%} / (\text{Ru} + \text{Os}) \text{ at. \%}$. b.d.l.—below the detection limit; the detection limits here and in Table 2 are as follows (wt.%): Os—0.15, Ir—0.75, Ru—0.24, Rh—0.01, Pt—0.09, Pd—0.27, Fe—0.15, Ni—18, Cu—0.15, S—0.13, As—0.01.

Table 2. Electron microprobe analyses of Ru-Os sulfides of type 2 and coexisting Os-Ir alloys from the Verkh-Neivinsk massif.

Analysis	10	11	12	13	14	15	16
Sample #	159	9	9	24	24	26	26
Mineral	(Os,Ir)	laurite	(Os,Ir)	laurite	(Os,Ir)	laurite	(Os,Ir)
Figure	Figure 3e	Figure 6a	Figure 6a	Figure 6b	Figure 6b	Figure 6c	Figure 6c
	wt. %						
Fe	b.d.l.	b.d.l.	b.d.l.	b.d.l.	b.d.l.	0.27	0.22
Ru	1.26	26.98	1.34	49.56	11.44	22.81	0.95
Rh	b.d.l.	b.d.l.	b.d.l.	0.25	0.15	0.12	b.d.l.
Os	89.13	36.92	83.82	11.44	77.51	36.99	57.26
Ir	9.38	4.54	14.66	1.83	10.49	8.28	41.55
S	b.d.l.	31.34	b.d.l.	36.95	b.d.l.	31.30	b.d.l.
Total	99.77	99.78	99.82	100.03	99.59	99.77	99.98
	at. %						
Fe	0.00	0.00	0.00	0.00	0.00	0.33	0.74
Ru	2.35	18.26	2.50	28.59	19.62	15.61	1.77
Rh	0.00	0.00	0.00	0.14	0.26	0.08	0.00
Os	88.44	13.28	83.12	3.51	70.66	13.45	56.75
Ir	9.21	1.62	14.38	0.56	9.46	2.98	40.74
S	0.00	66.84	0.00	67.20	0.00	67.55	0.00
Ru #		56		89		54	

(Os,Ir)—iridian osmium. Ru# = $100 \times \text{Ru at. \%} / (\text{Ru} + \text{Os}) \text{ at. \%}$. b.d.l.—below the detection limit; detection limit for concentrations in iridian osmium were as follows, wt.%: Os—0.18, Ir—0.85, Ru—0.27, Rh—0.11, Pt—0.99, Pd—0.30, Fe—0.16, Ni—0.18, Cu—0.15, S—0.06, As—0.03.

Table 3. Electron microprobe analyses of high-Mg olivine inclusions in osmian iridium and Ru-Os sulfides from primary PGM assemblage of the Verkh-Neivinsk massif.

Analysis	1	2	3	4	5	6	7	8	9
Sample #	8	164	164	164	154	154	154	165	165
Figure	Figure 4a	Figure 4b	Figure 4b	Figure 4b	Figure 4c	Figure 4c	Figure 4c	Figure 4d	Figure 4d
Host mineral	(Ir,Os)	LR	LR	LR	LR	LR	LR	LR	LR
wt.%									
SiO ₂	40.33	40.68	40.55	40.39	39.72	40.96	40.74	40.73	41.21
MgO	50.42	50.69	50.61	50.61	51.92	51.83	51.66	52.23	52.37
FeO	6.70	7.72	7.73	7.78	6.10	6.64	6.33	6.19	5.95
NiO	0.40	0.33	0.34	0.35	0.42	0.41	0.42	0.14	0.17
MnO	0.13	0.06	0.14	0.11	0.08	0.09	0.10	0.25	0.32
Total	97.98	99.48	99.37	99.24	98.24	99.93	99.25	99.54	100.02
Apfu				Cations on the basis of 4 O atoms					
Si	1.00	0.99	0.99	0.99	0.98	0.99	0.99	0.99	0.99
Mg	1.86	1.85	1.85	1.85	1.91	1.87	1.88	1.89	1.88
Fe ²⁺	0.14	0.16	0.16	0.16	0.13	0.14	0.13	0.13	0.12
Ni	0.01	0.01	0.01	0.01	0.01	0.01	0.01	0.00	0.00
Mn	0.00	0.00	0.00	0.00	0.00	0.00	0.00	0.01	0.01
Fo	93	92	92	92	94	93	94	94	94

(Ir,Os)—osmian iridium, LR—laurite, ERL—erlichmanite, (Ru,Os,Ir)—ruthenium; Al₂O₃, CaO, TiO₂, and Cr₂O₃ were below the detection limit, Fo = 100 × Mg/(Mg + Fe).

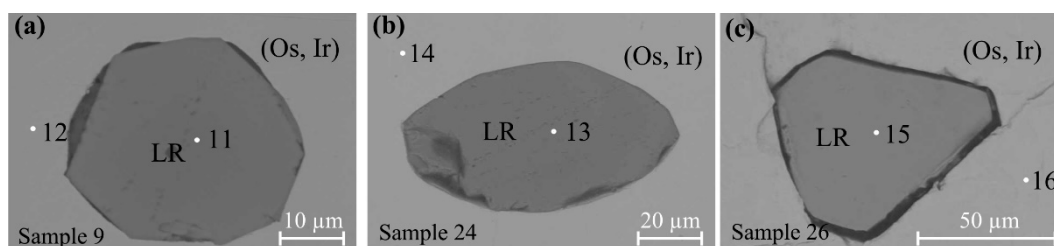


Figure 6. Back-scattered images of laurite grains of type 2 at Verkh-Neivinsk: (a)—sample 9, (b)—sample 24, (c)—sample 26. LR—laurite, (Os,Ir)—iridian osmium. Numbers 11–16 denote areas of electron microprobe analyses corresponding to the same numbers in Table 2.

Two morphological groups of Ru-Os sulfides were distinguished. The first one (type 1) includes single grains ranging in size from 1.0 to 1.5 mm (Figure 3a–e). They show a complete compositional spectrum, from laurite RuS₂ to erlichmanite OsS₂ (Figure 7a, Ru # varies from 12 to 89). In addition to Ru, Os, and S, these minerals have significant contents of Ir (3.32–10.71 wt.%) and negligible abundances of Fe, Ni, and Rh, which vary within 0.17–0.40, b.d.l.–0.23, and b.d.l.–0.39 wt.%, respectively (Table 1). Ru-Os sulfides contain inclusions of iridian osmium (Os, Ir) that can be as large as 30 μm across (Figure 3c,f and Table 2, analysis 10), and high-magnesian olivine (Fo_{92–94}) with grain sizes from 5 to 40 μm (Figures 4 and 5, Table 3, analyses 2–9). Ru-Os sulfides of the second morphological group (type 2) represent mineral inclusions (with typical sizes of 30–80 microns) enclosed in Os-Ir-(Ru) alloys (Figure 6, Table 2, analyses 12, 14, 16). These inclusions have higher ruthenium content (Figure 7b, Ru # varies from 54 to 100) and correspond to laurite (Table 2, analyses 11, 13, 15). Rare inclusions of high-magnesian olivine (Fo₉₃) were also revealed in Os-Ir alloy (Figure 4a, Table 3, analysis 1).

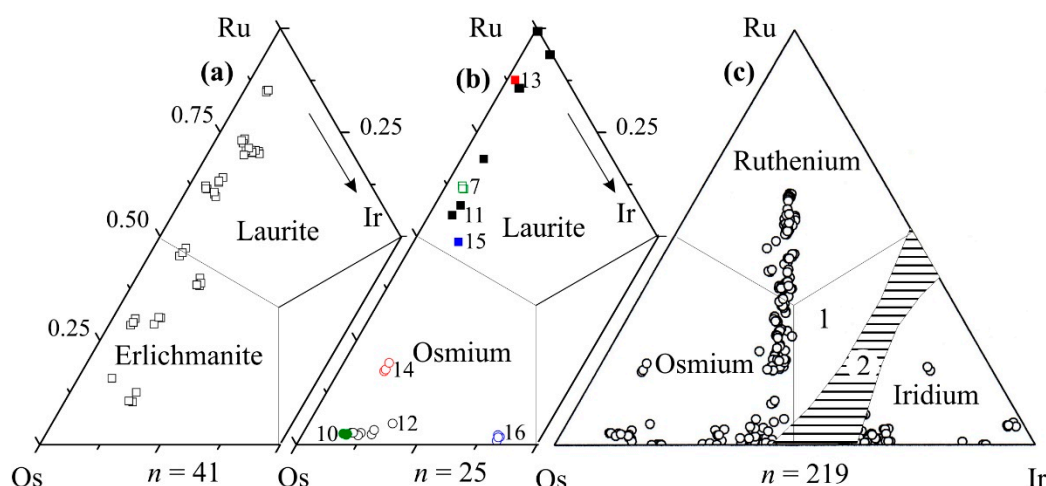


Figure 7. Chemical composition of: (a) Ru-Os sulfides type 1, (b) coexisting laurite type 2 and Os-rich alloy grains, (c) Ru-Os-Ir alloys from the Verkh-Neivinsk massif in coordinates Ru-Os-Ir (at.%). Numbers 7–16 in Figure 7b correspond to the same numbers of electron microprobe analyses in Tables 1 and 2. Squares and circles refer to laurite and Os alloy, respectively. Different symbol colors denote laurite–alloy pairs shown in Figure 3c,f and Figure 6. Numbers 1 and 2 in Figure 7c correspond to rutheniridosmine and miscibility gap, respectively (after nomenclature of Harris and Cabri [79]).

Os-Ir-Ru alloys from the primary PGM assemblage of Verkh-Neivinsk are dominated by native osmium, ruthenium, and iridium (Figure 7c). The variation of osmium and ruthenium concentrations are due to the substitution by iridium in the solid solution of osmium (the trend of compositions along the horizontal axis Os-Ir in Figure 7c) or ruthenium (vertical trend of compositions towards Ru, Figure 7c).

4.2. Sulfur Isotope Data

The $\delta^{34}\text{S}$ values in Ru-Os sulfides of both morphological types show a relatively narrow range from 0.3 to 3.3‰ (Table 4, Figures 8 and 9), with a mean of 2.05‰ and a standard deviation of 0.86‰ ($n = 18$). The $\delta^{34}\text{S}$ values in Ru-Os sulfides of type 1 have slightly narrower range from 0.3 to 2.8‰ (Table 4, Figure 10), with a mean of $1.82 \pm 0.83\text{‰}$ ($n = 14$). We note that the mean $\delta^{34}\text{S}$ value for laurite (i.e., $1.64 \pm 0.91\text{‰}$, $n = 9$) corresponds, within the analytical error, to that of erlichmanite ($2.16 \pm 0.55\text{‰}$, $n = 5$; Table 4, Figure 10). Laurite inclusions of type 2 are characterized by $\delta^{34}\text{S}$ composition ranging from 1.5 to 3.3‰ (Table 4, Figure 10) and a slightly higher $\delta^{34}\text{S}$ mean of $2.66 \pm 0.73\text{‰}$ ($n = 4$).

Table 4. Sulfur and osmium isotope data of Ru-Os sulfides and associated Os-rich alloys at Verkh-Neivinsk.

Sample Number, Figure	Mineral, Ru#	$^{187}\text{Os}/^{188}\text{Os}^*$	$1\sigma^*$	$^{187}\text{Re}/^{188}\text{Os}^*$	$\text{TRD}^{\text{ECR}*}$ (Ga)	1σ (Ga)	$\delta^{34}\text{S}, \text{‰}$
Ru-Os sulfides of type 1 and inclusions of iridian osmium							
153, Figure 8a	LR, 78	0.12135	0.00003	0.00002	0.955	0.004	2.5
154, Figure 8b	LR, 77	0.12381	0.00003	0.00009	0.609	0.004	2.0
156, Figure 3b	LR, 77	0.12386	0.00002	0.00003	0.602	0.003	2.2
157, Figure 8d	LR, 75	0.12201	0.00002	0.00005	0.863	0.002	2.2
159-1, Figures 3c and 8e	LR, 64	0.11728	0.00002	0.00001	1.523	0.003	2.6
159-2, Figures 3f and 8e	(Os,Ir)	0.11720	0.00009	0.00023	1.535	0.012	-

Table 4. Cont.

Sample Number, Figure	Mineral, Ru#	$^{187}\text{Os}/^{188}\text{Os}$ *	1σ *	$^{187}\text{Re}/^{188}\text{Os}$ *	$T_{\text{RD}}^{\text{ECR}*}$ (Ga)	1σ (Ga)	$\delta^{34}\text{S}$, ‰
163, Figure 8h	LR, 75	0.12503	0.00001	0.00003	0.436	0.002	1.9
164-1, Figure 8j	LR, 89	0.11946	0.00003	0.00004	1.219	0.004	0.5
164-2, Figure 8j	LR, 89	0.11943	0.00004	0.00002	1.223	0.005	0.6
165, Figure 8l	LR, 64	0.11889	0.00002	0.00006	1.298	0.002	0.3
155, Figure 8c	ERL, 32	0.12213	0.00002	0.00002	0.845	0.003	1.9
160, Figure 8f	ERL, 44	0.12788	0.00003	0.00006	0.029	0.005	1.7
161, Figure 8i	ERL, 12	0.13459	0.00002	0.00002	-	-	2.8
162, Figures 3d and 8g	ERL, 32	0.12261	0.00002	0.00003	0.778	0.002	1.7
166, Figures 3e and 8k	ERL, 49	0.12061	0.00001	0.00002	1.059	0.002	2.7
Ru-Os sulfides of type 2 and associated Os-rich alloys							
9, Figure 9a	LR, 56	0.12302	0.00003	0.00002	0.720	0.004	n/d
9, Figure 9a	(Os,Ir)	0.12306	0.00002	0.00009	0.714	0.003	-
24, Figure 9b	LR, 89	0.11774	0.00004	0.00001	1.459	0.006	3.1
24, Figure 9b	(Os,Ru,Ir)	0.11786	0.00002	0.00003	1.443	0.003	-
26, Figure 9c	LR, 54	0.12506	0.00002	0.00002	0.432	0.003	3.3
26, Figure 9c	(Os,Ir)	0.12512	0.00001	0.00036	0.423	0.002	-
71	LR, 89	0.12491	0.00003	0.00008	0.453	0.005	2.4
71	(Os,Ir,Ru)	0.12505	0.00002	0.00033	0.434	0.002	-
126	LR, 100	0.12410	0.00013	0.00019	0.568	0.018	1.5
194	LR, 100	0.11898	0.00009	0.00031	1.286	0.014	n/d
194	(Ru,Os,Ir)	0.11891	0.00003	0.00140	1.296	0.004	-

Ru# = $100 \times \text{Ru at.}\% / (\text{Ru} + \text{Os}) \text{ at.}\%$. *—data after Reference [50], except sample numbers 160 and 126. $T_{\text{RD}}^{\text{ECR}}$ values estimated by Walker et al. [74] and a decay constant of $\lambda = 1.666 \times 10^{-11} \text{ year}^{-1}$ [73]. Uncertainties on model ages are based on within-run errors only. LR—laurite; ERL—erlichmanite; (Os,Ir), (Os, Ru, Ir), (Os,Ir,Ru)—osmium; (Ru,Os,Ir)—ruthenium, n/d—not determined.

4.3. Osmium Isotope Data

The Os-isotope data for Ru-Os sulfides and associated Os-rich alloys are provided in Table 4 and Figures 8 and 9. Solitary grains of laurite and erlichmanite of type 1 show a very wide range of $^{187}\text{Os}/^{188}\text{Os}$ values (between 0.11728 and 0.13459, and $^{187}\text{Re}/^{188}\text{Os} < 0.00009$). $^{187}\text{Os}/^{188}\text{Os}$ values in laurite and erlichmanite vary from 0.11728 to 0.12503 and from 0.12061 to 0.13459, respectively (Table 4). Thus, in addition to sub-chondritic values ($^{187}\text{Os}/^{188}\text{Os} < 0.1281$), a supra-chondrite isotope composition of osmium was detected in erlichmanite ($^{187}\text{Os}/^{188}\text{Os} = 0.13459 \pm 0.00002$). If the outliers with the most radiogenic $^{187}\text{Os}/^{188}\text{Os}$ values in erlichmanite grains are excluded (i.e., 0.12788 and 0.13459, respectively), the Os-isotope results identify a more restricted $^{187}\text{Os}/^{188}\text{Os}$ range for erlichmanite (0.12061–0.12261) of the first morphological type. Laurite inclusions typical of the second morphological type are characterized by a similar degree of Os-isotope variations ($^{187}\text{Os}/^{188}\text{Os}$ from 0.11774 to 0.12506, Table 4, Figure 9) with that of type 1 laurites. We also note a similarity of the Os-isotopic compositions for coexisting laurite and Os-Ir-(Ru) alloys (Table 4, Figure 9a,b).

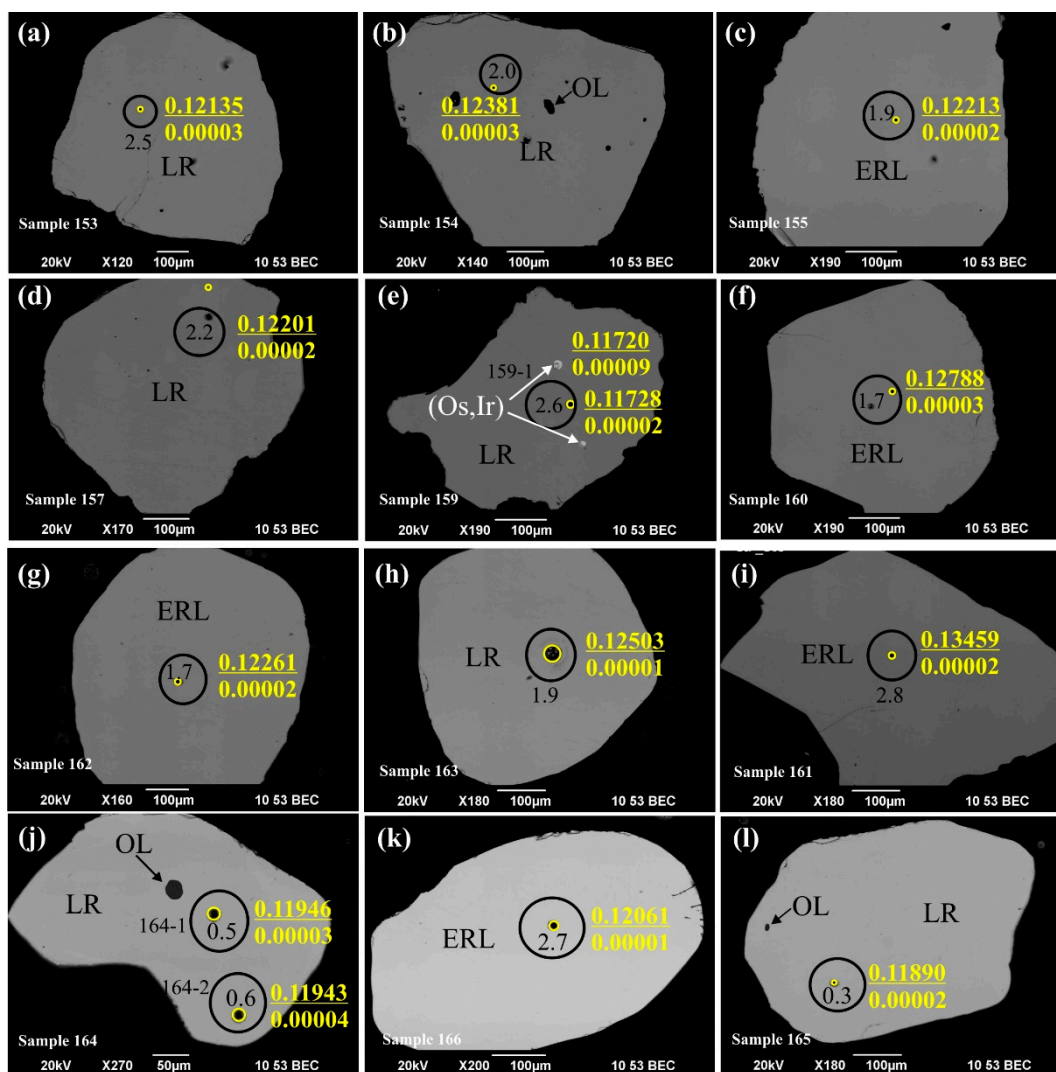


Figure 8. Back-scattered electron images of Ru-Os sulfides type 1 at Verkh-Neivinsk: (a)—sample 153, (b)—sample 154, (c)—sample 155, (d)—sample 157, (e)—sample 159, (f)—sample 160, (g)—sample 162, (h)—sample 163, (i)—sample 161, (j)—sample 164, (k)—sample 166, (l)—sample 165. Yellow circles with a diameter of 15–40 μm denote areas of Os-isotope analyses listed in Table 4. Yellow numerals in the numerator and denominator correspond to the $^{187}\text{Os}/^{188}\text{Os}$ value and the measurement error, respectively. Black circles with a diameter ca. 100 μm denote spots of S-isotope analyses listed in Table 4. The numbers correspond to the $\delta^{34}\text{S}$ (‰) value. LR—laurite, ERL—erlichmanite, (Os, Ir)—iridian osmium, OL—high-Mg olivine.

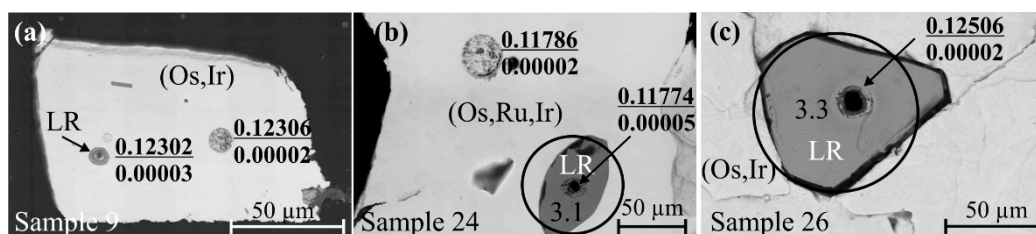


Figure 9. Back-scattered electron images of Ru-Os sulfides type 2 and associated Os-rich alloys at Verkh-Neivinsk: (a)—sample 9, (b)—sample 24, (c)—sample 26. “Craters” with a diameter of 15–40 μm denote areas of Os-isotope analyses listed in Table 4. The numerals in the numerator and denominator correspond to the $^{187}\text{Os}/^{188}\text{Os}$ value and the measurement error, respectively. Black circles with a diameter ca. 100 μm denote spots of S-isotope analyses listed in Table 4. LR—laurite, (Os, Ir)—iridian osmium, (Os, Ru, Ir)—osmium.

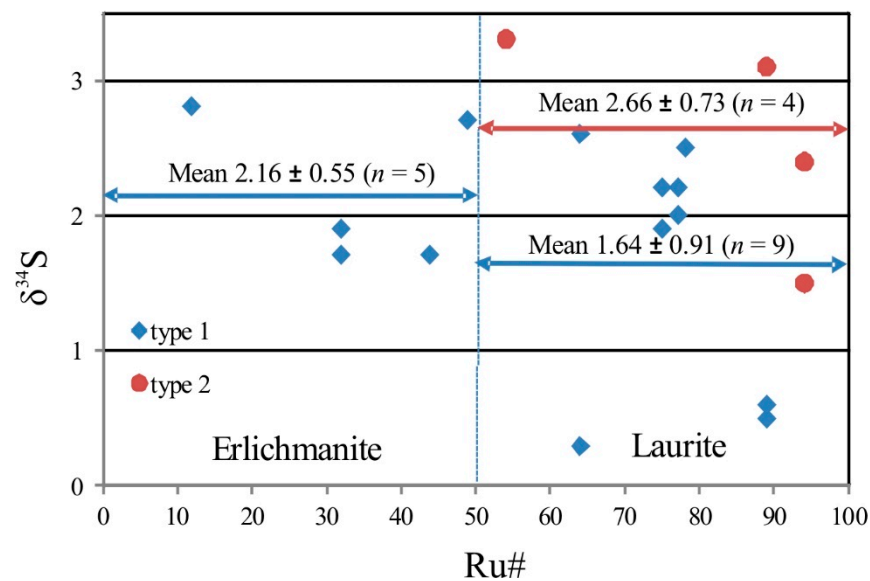


Figure 10. Sulfur isotope data for Ru-Os sulfides of type 1 and 2 within primary PGM assemblage from the Verkh-Neivinsk massif.

Due to very low $^{187}\text{Re}/^{188}\text{Os}$ values, the Re-Os model and Re-depletion ages (i.e., T_{MA} and T_{RD} [71,72]) of Ru-Os sulfides are identical. T_{RD} ages for laurite of the first and second type, calculated relative to an Enstatite Chondrite Reservoir (ECR) model [74], display comparable variations (436–1523 and 432–1459 Ma respectively, Table 4), whereas erlichmanites are characterized by more moderate variations (T_{RD} ages from 1059 to 778 Ma).

5. Discussion

The provenance of the investigated Ru-Os sulfide and Ru-Os-Ir alloy grains is obvious: the placer deposits display a close spatial association with the Verkh-Neivinsk dunite-harzburgite massif (Figure 2). The primary nature of Ru-Os sulfides of the first morphological type is supported by occurrence of euhedral inclusions of high-Mg olivine (Fo_{92-94}) that fall within the compositional range of mantle (primitive) olivine (Fo_{88-93}) and also perfectly match the composition of olivine (with a pronounced peak between Fo_{93} and Fo_{94}) in peridotite xenoliths from the mantle beneath Archean cratons [80–82]. The primary PGM from chromitites that form relatively small discordant bodies in residual dunites and harzburgites at Verkh-Neivinsk (unpublished data) share mineralogical and compositional characteristics with those of the detrital PGM. These chromitites are characterized by negatively sloped, chondrite-normalized platinum-group element (PGE) patterns [83], which is consistent with the preponderance of a rather limited variety of PGM of the IPGE group (i.e., dominated by laurite and Ru-Os-Ir alloy). Based on these lines of evidence, we suggest that the studied Ru-Os sulfides were derived from mantle residual rocks of the Verkh-Neivinsk massif, although the derivation of these PGM from the Moho-transition zone dunite-clinopyroxenite complex cannot be ruled out. Both options may be verified by distinct Ni concentrations in highly-magnesian olivine inclusions within the studied PGM. High Ni contents (0.33–0.42 wt.%) in all but one forsterite inclusions are consistent with a mantle origin of olivine, whereas moderate Ni abundances (0.14–0.17 wt.%) in forsterite within Os-rich laurite may indicate its derivation from different source rocks that form dunite-clinopyroxenite complex.

The composition of the laurite-erlichmanite series, plotted on the Os-Ir-Ru diagram (Figure 7a), shows common Os substitution for Ru (Ru# between 12 and 89), typical of mantle chromitites from Kempirsai and Rai-Iz (Urals), Kraubath, Eastern Alps, and Unst, Shetland Isles [5,9,11,84]. A high-temperature origin of euhedral inclusions of laurite type 2 in Os-Ir-(Ru) alloys are supported by recent experimental data [18–21] that quantitatively

evaluated the effects of T and $f(S_2)$ for laurite + alloy mineral pairs. This is consistent with the presence of a ruthenium trend in Ru-Os-Ir alloys at Verkh-Neivinsk (Figure 7c), which is indicative of high temperature and pressure values that can only be reached under mantle conditions [85]. These integrated data present irrefutable evidence that Os-Ir-Ru alloys have formed at high T-P environments and that the observed chemical compositional variations represent primary features of the grains [26,40,42,70,85–88]. Thus, these refractory alloys are considered to be representative of depleted mantle material within the mantle sections of ophiolites.

The early formation of laurite and Os-Ir alloys at high T-P conditions implies that the original S- and Os-isotope composition of these PGM reflects the source region in the mantle at the time of their formation. The sulfur-isotope results of this study display a narrow range of $\delta^{34}\text{S}$ values for single (individual) type 1 laurite grains ranging from 0.3 to 2.8, with a mean of 1.64‰ and a standard deviation of 0.91‰ ($n = 9$), which is within the analytical uncertainty with that of solitary erlichmanite grains ($\delta^{34}\text{S}$ mean of $2.16 \pm 0.55\%$, $n = 5$) and laurite inclusions of type 2 ($\delta^{34}\text{S}$ mean of $2.66 \pm 0.73\%$, $n = 4$, Figure 10). According to Thode et al. [89], the sulfur isotope composition of the Earth's mantle is considered to be homogeneous with a mean $\delta^{34}\text{S}$ of 0.0‰, a value indistinguishable from that of chondrites ($\delta^{34}\text{S} = 0.04 \pm 0.31\%$, $n = 24$ [90,91]). Delta ^{34}S values beyond $0 \pm 2\%$ are considered to be a result of the mantle–crust interaction processes (denoting a contribution of crustal-derived sulfur) both at mantle conditions [92] and during formation of mantle magmas under crustal conditions [93]. The sulfur isotope composition of Ru-Os sulfides from the oceanic mantle was initially studied by Hattori et al. [24], who showed that Ru-Os sulfides from placer deposits in Borneo have a mean $\delta^{34}\text{S}$ value of $1.16 \pm 0.36\%$, which is consistent with a mantle source of sulfur. In a subsequent investigation of solitary grains of Ru-Os sulfides at Verkh-Neivinsk ($\delta^{34}\text{S} = 1.29 \pm 0.65\%$) [51], they appeared to be similar to that of Ru-Os sulfides from placers in Borneo [24]. Our S-isotope study of two morphological types (i.e., individual Ru-Os sulfide grains and laurite inclusions in Os-Ir-(Ru) alloys representing the primary PGM assemblage at Verkh-Neivinsk) is indicative of a sub-chondritic source of sulfur. This conclusion is consistent with the osmium isotope data obtained for Os-bearing PGM from the Verkh-Neivinsk massif (Middle Urals). The considerable range of the sub-chondritic $^{187}\text{Os}/^{188}\text{Os}$ values in Ru-Os sulfides (0.11728–0.12788, $n = 19$, Figure 11) and Ru-Os-Ir alloys (0.11619–0.12270, $n = 34$, Figure 11) are clearly indicative of derivation from a sub-chondritic source. This wide $^{187}\text{Os}/^{188}\text{Os}$ range, with rare exceptions [35,63], is similar to that of the PGM from podiform chromitites within the mantle sections of dunite-harzburgite massifs and associated placer deposits (Figure 11, see also Figure 11 in Reference [36]). On the other hand, the osmium isotope data display a restricted range of sub-chondritic $^{187}\text{Os}/^{188}\text{Os}$ values for intimately intergrown laurite type 2 and Os-rich alloy pairs that form the primary PGM assemblage (Figure 9a,b). In such pairs, the Os-isotope signature of the adjacent phases is indistinguishable. This is consistent with similar findings for PGM from Witwatersrand, South Africa [42], Shetland, Scotland [35], and Hochgrossen, Eastern Alps, Austria [49].

A single value of $^{187}\text{Os}/^{188}\text{Os} = 0.13459 \pm 0.00002$ identified in the erlichmanite indicates derivation from the source that evolved with long-term supra-chondritic Re/Os. This feature can be interpreted as evidence of a radiogenic crustal component, which was introduced during a subduction-related event or alternatively as an indication of an enriched mantle source. Consequently, supra-chondritic $^{187}\text{Os}/^{188}\text{Os}$ values (>0.12810), which have also been identified in detrital Os-Ir-(Ru) alloy grains [30,58,94,95], may indicate derivation from a distinct source, which is different from that of residual dunite-harzburgite sequences of an ophiolite complex. Distinct sources of HSE have recently been confirmed for Os-rich alloys derived from different lithologies (i.e., chromitite and clinopyroxenite) of the Kondyor massif [66] that was advocated to have trans-lithospheric mantle origin [96,97].

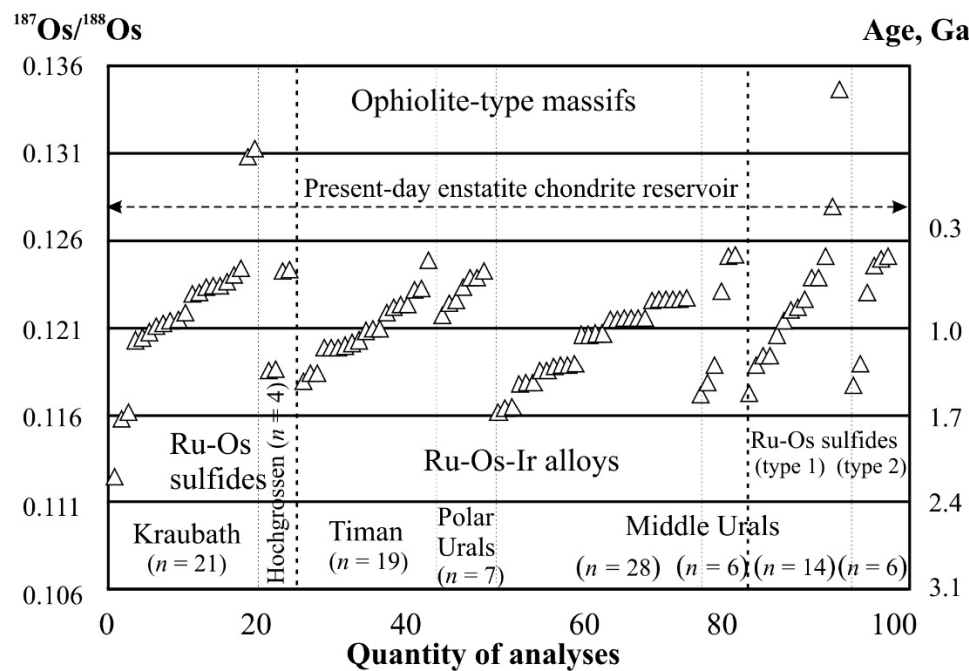


Figure 11. Os-isotopic composition of Ru-Os sulfides and Ru-Os-Ir alloys of dunite-harzburgite massifs. Os-isotopic data for Ru-Os sulfides of the Kraubath and Hochgrossen massifs (Eastern Alps) and Ru-Os-Ir alloys from the Timan, Polar, and Middle Urals according to References [39,49,56]. Present-day enstatite chondrite reservoir after Reference [74].

The time of formation of the oceanic crust in the Uralian ophiolites is usually ascribed to Early Devonian to Middle Ordovician (about 390 to 470 Ma) by Sm-Nd mineral and whole-rock isochrons on ultramafic rocks and gabbros from the Kempirsai massif [98,99] and by U-Pb dating of zircon from rock lithologies of the Vostochny Tagil (Middle Urals) and Nurali (South Urals) ultramafic complexes [100,101]. With the exception of two outliers (samples 160 and 161), the obtained T_{RD} ages of Ru-Os sulfides at Verkh-Neivinsk imply that the mantle domain under Middle Urals experienced melt extraction between 1525 and 435 Ma (Table 4, Figure 12). The Os isotopic compositions of these PGM indicate that they record much older melting events than it would be expected from a single-melting model of un-depleted mantle around 440 Ma. One of the explanations of this phenomenon is that after their formation, Ru-Os sulfides remained isolated from the convecting upper mantle. In this case, ultramafic rocks of the Verkh-Neivinsk massif do not represent a simple residue after partial melting at a mid-ocean ridge setting or evolved back-arc system in the Early Paleozoic. Instead, they may represent a mixture of (1) refractory isolated lithospheric blocks that retain much older ages and (2) ultramafic rocks formed during a partial melting episode in the Early Paleozoic. A similar scenario has been advocated by Parkinson et al. [102] and Snow and Schmidt [103] for the Izu-Bonina-Mariana and Zabargad peridotites, respectively. Osmium isotope systematics suggest that melt depletion events recorded by un-radiogenic $^{187}\text{Os}/^{188}\text{Os}$ at Verkh-Neivinsk (Figure 11) and some other peridotite occurrences worldwide, e.g., References [59,62,102,103], etc., are significantly older than the time of their emplacement into crustal levels. This observation is similar to the phenomenon recorded by Re-Os isotopes in sulfide inclusions in diamonds [104]. Variations in the T_{RD} ages of PGM at Verkh-Neivinsk point to prolonged melt-extraction processes and likely multi-stage evolution of HSE within the upper mantle. This is consistent with statistically significant data for Ru-Os-Ir alloys from the dunite-harzburgite massifs of the Urals [39] that show several stages of PGM formation with an average cycle of 150–200 Ma. This variability is likely to be due to discrete mantle melting events, which are probably controlled by deep mantle geodynamic processes [105]. The observed coincidence between the T_{RD} ages of PGM and U-Pb ages of zircon recovered from the ultramafic massifs of the Urals [39,59,98,106–109] provides a feasible evidence of close relationships between magmatic and ore-forming processes.

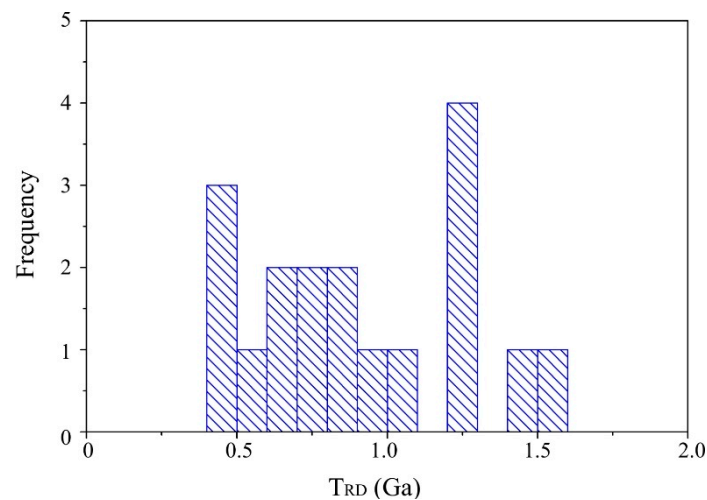


Figure 12. Histogram of mantle-depletion (T_{RD}) ages of Ru-Os sulfides at Verkh-Neivinsk.

6. Conclusions

1. A multi-technique approach, including the use of in-situ analytical methods for geochemical and isotopic analysis, provided a new set of mineralogical and S-Os isotope-geochemical constraints on the origin of detrital Ru-Os sulfides from primary PGM assemblage of the Verkh-Neivinsk ophiolite-type massif.
2. Ru-Os sulfides are recognized within two morphological types, including (i) solitary Ru-Os sulfide grains that have sizes from 0.5 to 1.5 mm and a wide compositional range for the laurite (RuS_2)–erlichmanite (OsS_2) solid solution series, and (ii) tiny euhedral inclusions of laurite hosted by Os-Ir(Ru) alloys. The primary nature of Ru-Os sulfides is supported by the occurrence of euhedral inclusions of high-Mg olivine (Fo_{92-94}) that fall within the compositional range of mantle (primitive) olivine (Fo_{88-93}).
3. The $\delta^{34}\text{S}$ values in solitary Ru-Os sulfide grains of type 1 have a narrow range from 0.3 to 2.8‰, with a mean of $1.82 \pm 0.83\text{‰}$ ($n = 14$), corresponding, within an error, to that for laurite inclusions of type 2 characterized by $\delta^{34}\text{S}$ variations ranging from 1.5 to 3.3‰ and a slightly higher $\delta^{34}\text{S}$ mean of $2.66 \pm 0.73\text{‰}$ ($n = 5$). The similar sub-chondritic $\delta^{34}\text{S}$ values reported for the detrital Ru-Os sulfides of the oceanic mantle origin [24,51] is consistent with derivation of sulfur from a sub-chondritic source.
4. The osmium isotope results identified two distinct sources of HSE for Ru-Os sulfides. A considerable range of the sub-chondritic $^{187}\text{Os}/^{188}\text{Os}$ values in Ru-Os sulfides (0.1173–0.1278, $n = 18$ [50], this study) and Ru-Os-Ir alloys (0.1162–0.1227, $n = 34$ [49], this study) clearly indicate a common near-chondritic source for the HSE.
5. The osmium isotope data display a restricted range of sub-chondritic $^{187}\text{Os}/^{188}\text{Os}$ values for intimately intergrown laurite type 2 and Os-rich alloy pairs that form the primary PGM assemblage. This is consistent with similar findings for PGM from Witwatersrand, South Africa [42], Shetland, Scotland [35], and Hochgrosven, Austria [49].
6. A single value of $^{187}\text{Os}/^{188}\text{Os} = 0.13459 \pm 0.00002$ identified in the erlichmanite indicated derivation from the source that evolved with a long-term supra-chondritic Re/Os. This feature may be interpreted as evidence of a radiogenic crustal component, which was introduced during a subduction-related event or an indication of an enriched mantle source. Consequently, supra-chondritic $^{187}\text{Os}/^{188}\text{Os}$ values (>0.12810) may indicate derivation from a distinct source other than residual dunite–harzburgite sequences of an ophiolite complex.
7. With the exception of two outliers (samples 160 and 161), the obtained T_{RD} ages of Ru-Os sulfides at Verkh-Neivinsk imply that the mantle domain under Middle Urals

experienced melt extraction between 1525 and 435 Ma, and they record much older melting events than would be expected from a single-melting model of un-depleted mantle around 440 Ma. We suggest that variations in the T_{RD} ages of the Verkh-Neivinsk PGM point to prolonged melt-extraction processes and likely multi-stage evolution of HSE within the upper mantle.

Author Contributions: This work included contributions from all the authors. K.N.M., I.Y.B., E.A.B., V.V.M. and T.A.V. took part in analytical work, discussing the data, writing and revising the manuscript. All authors have read and agreed to the published version of the manuscript.

Funding: This study was supported by Ministry of Science and Higher Education of the Russian Federation (state assignment # AAAA-A18-118052590026-5) and Russian Foundation for Basic Research (grant 18-05-00988-a to Inna Badanina).

Acknowledgments: The manuscript has benefitted from constructive comments of three anonymous reviewers and careful handling and editorial input by Editor Mauricio Calderón. The analytical work at CCFS/GEMOC was funded by DEST Systemic Infrastructure—Department of Education, Science and Training Systemic Infrastructure (Australia) Grants, ARC LIEF, NCRIS, industry partners, and Macquarie University. We thank Vera Khiller and Vladislav Bulatov for help in the microprobe lab. This is contribution 1614 from the ARC Centre of Excellence for Core to Crust Fluid Systems and 1436 in the GEMOC Key Centre. The Os-isotope data were obtained using instrumentation funded by DEST Systemic Infrastructure Grants, ARC LIEF, NCRIS/AuScope, industry partners and Macquarie University.

Conflicts of Interest: The authors declare no conflict of interest.

References

1. Augé, T. Platinum-group-mineral inclusions in ophiolitic chromite from the Vourinos Complex, Greece. *Can. Mineral.* **1985**, *23*, 163–171.
2. Augé, T. Platinum-group minerals in the Tiebaghi and Vourinos ophiolitic complexes: Genetic implications. *Can. Mineral.* **1988**, *26*, 177–192.
3. Rudashevsky, N.S. Platinum-Group Elements in Rocks of Ultramafic Formations (Mineralogy and Genesis). Habil. Thesis, Mining Institute, Leningrad, Russia, 1989. (In Russian).
4. Cabri, L.-J.; Harris, D.C.; Weiser, T.W. Mineralogy and distribution of platinum-group mineral (PGM) placer deposits of the world. *Explor. Min. Geol.* **1996**, *5*, 73–167.
5. Garuti, G.; Zaccarini, F.; Moloshag, V.; Alimov, V. Platinum-group minerals as indicators of sulfur fugacity in ophiolitic upper mantle: An example from chromitites of the Rai-Iz ultramafic complex, Polar Urals, Russia. *Can. Mineral.* **1999**, *37*, 1099–1115.
6. Melcher, F. Chromite and Platinum-Group Elements as Indicators of Mantle Petrogenesis. Mining University of Leoben, Leoben, Austria, 2000. Unpublished Habil Thesis.
7. Zaccarini, F.; Pushkarev, E.; Garuti, G. Platinum-group element mineralogy and geochemistry of chromitite of the Kluchevskoy ophiolite complex, central Urals (Russia). *Ore Geol. Rev.* **2008**, *33*, 20–30. [[CrossRef](#)]
8. Zaccarini, F.; Pushkarev, E.; Garuti, G.; Kazakov, I. Platinum-group minerals and other accessory phases in chromite deposits of the Alapaevsk ophiolite, Central Urals, Russia. *Minerals* **2016**, *6*, 108. [[CrossRef](#)]
9. Malitch, K.N.; Thalhhammer, O.A.R.; Knauf, V.V.; Melcher, F. Diversity of platinum-group mineral assemblages in banded and podiform chromitite from the Kraubath ultramafic massif, Austria: Evidence for an ophiolitic transition zone? *Miner. Depos.* **2003**, *38*, 282–297. [[CrossRef](#)]
10. González-Jiménez, J.M.; Gervilla, F.; Proenza, J.A.; Augé, T.; Kerestedjian, T. Distribution of platinum-group minerals in ophiolitic chromitites. *Appl. Earth Sci.* **2010**, *118*, 101–110. [[CrossRef](#)]
11. Badanina, I.Y.; Malitch, K.N.; Lord, R.A.; Meisel, T.C. Origin of primary PGM assemblage in chromitite from a mantle tectonite at Harold's Grave (Shetland Ophiolite Complex, Scotland). *Mineral. Petrol.* **2013**, *107*, 963–970. [[CrossRef](#)]
12. González-Jiménez, J.M.; Griffin, W.L.; Gervilla, F.; Proenza, J.A.; O'Reilly, S.Y.; Pearson, N.J. Chromitites in ophiolites: How, where, when, why? Part I. A review and new ideas on the origin and significance of platinum-group minerals. *Lithos* **2014**, *189*, 127–139. [[CrossRef](#)]
13. Kiseleva, O.N.; Zhmodik, S.M.; Damdinov, B.B.; Agafonov, L.V.; Belyanin, D.K. Composition and evolution of PGE mineralization in chromite ores from the Il'chir ophiolite complex (Ospa-Kitoy and Khara-Nur areas, East Sayan). *Russ. Geol. Geophys.* **2014**, *55*, 259–272. [[CrossRef](#)]
14. O'Driscoll, B.; González-Jiménez, J.M. Petrogenesis of the platinum-group minerals. *Rev. Mineral. Geochem.* **2016**, *81*, 489–578. [[CrossRef](#)]

15. Kiseleva, O.; Zhmodik, S. PGE mineralization and melt composition of chromitites in Proterozoic ophiolite complexes of Eastern Sayan, Southern Siberia. *Geosci. Front.* **2017**, *8*, 721–731. [[CrossRef](#)]
16. Massalski, T.B.; Murray, J.L.; Bennet, L.H.; Baker, H. *Binary Alloy Phase Diagrams*; American Society for Metals: Russel Township, OH, USA, 1993; 2224p.
17. Amosse, J.; Dable, P.; Allibert, M. Thermochemical behaviour of Pt, Ir, Rh, and Ru vs fO_2 and fS_2 in a basaltic melt. Implications for the differentiation and precipitation of these elements. *Miner. Pet.* **2000**, *68*, 29–62.
18. Andrews, D.R.A.; Brenan, J.M. Phase-equilibrium constraints on the magmatic origin of laurite + Ru–Os–Ir alloy. *Can. Miner.* **2002**, *40*, 1721–1735. [[CrossRef](#)]
19. Brenan, J.M.; Andrews, D. High-temperature stability of laurite and Ru–Os–Ir alloy and their role in PGE fractionation in mafic magmas. *Can. Mineral.* **2001**, *39*, 341–360. [[CrossRef](#)]
20. Fonseca, R.O.C.; Laurenz, V.; Mallmann, G.; Luguët, A.; Hoehne, N.; Jochum, K.P. New constraints on the genesis and long-term stability of Os-rich alloys in the Earth’s mantle. *Geochim. Cosmochim. Acta* **2012**, *87*, 227–242. [[CrossRef](#)]
21. Fonseca, R.O.C.; Brückel, K.; Bragagni, A.; Leitzke, F.P.; Speelmanns, I.M.; Wainwright, A.N. Fractionation of rhenium from osmium during noble metal alloy formation in association with sulfides: Implications for the interpretation of model ages in alloy-bearing magmatic rocks. *Geochim. Cosmochim. Acta* **2017**, *216*, 184–200. [[CrossRef](#)]
22. Badanina, I.Y.; Zharkova, E.V.; Kadik, A.A.; Malitch, K.N.; Murzin, V.V. Results of experimental determination of the intrinsic oxygen fugacity of Ru–Os–Ir alloys from the Verkh-Neivinsky dunite-harzburgite massif, Middle Urals, Russia. *Geochem. Int.* **2015**, *53*, 658–663. [[CrossRef](#)]
23. González-Jiménez, J.M.; Gervilla, F.; Proenza, J.A.; Kerestedjian, T.; Augé, T.; Bailly, L. Zoning of laurite (RuS₂)-erlichmanite (OsS₂): Implications for the genesis of PGM in ophiolite chromitites. *Eur. J. Mineral.* **2009**, *21*, 419–432. [[CrossRef](#)]
24. Hattori, K.H.; Cabri, L.J.; Johanson, B.; Zientek, M.L. Origin of placer laurite from Borneo: Se and As contents, and S isotopic compositions. *Mineral. Mag.* **2004**, *68*, 353–368. [[CrossRef](#)]
25. Hattori, K.; Hart, S.R. Osmium-isotope ratios of platinum-group minerals associated with ultramafic intrusions: Os-isotopic evolution of the oceanic mantle. *Earth Planet. Sci. Lett.* **1991**, *107*, 499–514. [[CrossRef](#)]
26. Hattori, K.; Cabri, L.J. Origin of platinum-group mineral nuggets inferred from an osmium-isotope study. *Can. Mineral.* **1992**, *30*, 289–301.
27. Shi, R.; Alard, O.; Zhi, X.; O’Reilly, S.Y.; Pearson, N.J.; Griffin, W.L.; Zhang, M.; Chen, X. Multiple events in the Neo-Tethyan oceanic upper mantle: Evidence from Ru–Os–Ir alloys in the Luobusa and Dongqiao ophiolitic podiform chromitites, Tibet. *Earth Planet. Sci. Lett.* **2007**, *261*, 33–48. [[CrossRef](#)]
28. Malitch, K.N.; Junk, S.A.; Thallhammer, O.A.R.; Melcher, F.; Knauf, V.V.; Pernicka, E.; Stumpfl, E.F. Laurite and ruarsite from podiform chromitites at Kraubath and Hochgrussen, Austria: New insights from osmium isotopes. *Can. Mineral.* **2003**, *41*, 331–352. [[CrossRef](#)]
29. Ahmed, A.H.; Hanghøj, K.; Kelemen, P.B.; Hart, S.R.; Arai, S. Osmium isotope systematics of the Proterozoic and Phanerozoic ophiolitic chromitites: In-situ ion probe analysis of primary Os-rich PGM. *Earth Planet. Sci. Lett.* **2006**, *245*, 777–791. [[CrossRef](#)]
30. Pearson, D.G.; Parman, S.W.; Nowell, G.M. A link between large mantle melting events and continent growth seen in osmium isotopes. *Nature* **2007**, *449*, 202–205. [[CrossRef](#)] [[PubMed](#)]
31. Nowell, G.M.; Pearson, D.G.; Parman, S.W.; Luguët, A.; Hanski, E. Precise and accurate ¹⁸⁶Os/¹⁸⁸Os and ¹⁸⁷Os/¹⁸⁸Os measurements by Multi-collector Plasma Ionisation Mass Spectrometry, part II: Laser ablation and its application to single-grain Pt–Os and Re–Os geochronology. *Chem. Geol.* **2008**, *248*, 394–426. [[CrossRef](#)]
32. Marchesi, C.; González-Jiménez, J.M.; Gervilla, F.; Griffin, W.L.; O’Reilly, S.Y.; Proenza, J.A.; Pearson, N.J. In situ Re–Os isotopic analysis of platinum-group minerals from the Mayarí-Cristal ophiolitic massif (Mayarí-Baracoa Ophiolitic Belt, eastern Cuba): Implications for the origin of Os-isotope heterogeneities in podiform chromitites. *Contrib. Mineral. Petrol.* **2011**, *161*, 977–990. [[CrossRef](#)]
33. González-Jiménez, J.M.; Griffin, W.L.; Gervilla, F.; Kerestedjian, T.N.; O’Reilly, S.Y.; Proenza, J.A.; Pearson, N.J.; Sergeeva, I. Metamorphism disturbs the Re–Os signatures of platinum-group minerals in ophiolite chromitites. *Geology* **2012**, *40*, 659–662. [[CrossRef](#)]
34. González-Jiménez, J.M.; Locmelis, M.; Belousova, E.; Griffin, W.; Gervilla, F.; Kerestedjian, T.N.; O’Reilly, S.Y.; Pearson, N.J.; Sergeeva, I. Genesis and tectonic implications of podiform chromitites in the metamorphosed ultramafic massif of Dobromirtsi (Bulgaria). *Gondwana Res.* **2015**, *27*, 555–574. [[CrossRef](#)]
35. Badanina, I.Y.; Malitch, K.N.; Lord, R.A.; Belousova, E.A.; Meisel, T.C. Closed-system behaviour of the Re–Os isotope system recorded in primary and secondary PGM assemblages: Evidence from a mantle chromitite at Harold’s Grave (Shetland ophiolite Complex, Scotland). *Ore Geol. Rev.* **2016**, *75*, 174–185. [[CrossRef](#)]
36. González-Jiménez, J.M.; Mondal, S.K.; Ghosh, B.; Griffin, W.L.; O’Reilly, S.Y. Re–Os isotope systematics of sulfides in chromitites and host lherzolites of the Andaman ophiolite, India. *Minerals* **2020**, *10*, 686. [[CrossRef](#)]
37. Kostoyanov, A.I. Model Re–Os ages of platinum-group minerals. *Geol. Rudn. Mestorozhdenii* **1998**, *40*, 545–550. (In Russian)
38. Malitch, K.N.; Auge, T.; Badanina, I.Y.; Goncharov, M.M.; Junk, S.A.; Pernicka, E. Os-rich nuggets from Au–PGE placers of the Maimecha-Kotui Province, Russia: A multi-disciplinary study. *Mineral. Petrol.* **2002**, *76*, 121–148. [[CrossRef](#)]
39. Kostoyanov, A.I.; Ivanov, D.Y.; Manoilov, V.V. Polycyclic formation of platinum-group minerals from placers of the Ural and Timan. *Geochem. Int.* **2003**, *41*, 534–544.

40. Malitch, K.N.; Merkle, R.K.W. Ru-Os-Ir-Pt and Pt-Fe alloys from the Evander Goldfield (Witwatersrand Basin, South Africa): Detrital origin inferred from compositional and osmium isotope data. *Can. Mineral.* **2004**, *42*, 631–650. [[CrossRef](#)]
41. Pašava, J.; Malec, J.; Griffin, W.L.; González-Jiménez, J.M. Re-Os isotopic constraints on the source of platinum-group minerals (PGMs) from the Vestřev pyrope-rich garnet placer deposit, Bohemian Massif. *Ore Geol. Rev.* **2015**, *68*, 117–126. [[CrossRef](#)]
42. Badanina, I.Y.; Malitch, K.N.; Merkle, R.K.W.; Antonov, A.V.; Kapitonov, I.N.; Khiller, V.V. Chemical and isotopic composition of Os-rich alloys and sulfide from the Evander Goldfield of the Witwatersrand Basin (South Africa). *Lithosphere* **2016**, *16*, 129–144. (In Russian)
43. Dijkstra, A.H.; Dale, C.W.; Oberthür, T.; Nowell, G.M.; Pearson, D.G. Osmium isotope compositions of detrital Os-rich alloys from the Rhine River provide evidence for a global late Mesoproterozoic mantle depletion event. *Earth Planet. Sci. Lett.* **2016**, *452*, 115–122. [[CrossRef](#)]
44. González-Jiménez, J.M.; Griffin, W.L.; Proenza, J.A.; Gervilla, F.; O'Reilly, S.Y.; Akbulut, M.; Pearson, N.J.; Arai, S. Chromitites in ophiolites: How, where, when, why? Part II. The crystallisation of chromitites. *Lithos* **2014**, *189*, 140–158. [[CrossRef](#)]
45. Murzin, V.V.; Sustavov, S.G.; Mamin, N.A. *Gold and Platinum-Group Element Mineralization of Placer Deposits of the Verkh-Neivinskii Massif of Alpine Type Ultrabasites (Middle Urals)*; Ural State Mining University: Yekaterinburg, Russia, 1999; p. 93. (In Russian)
46. Volchenko, Y.A.; Koroteev, V.A.; Neustroeva, I.I. Platinum-group elements in Alpine-type ultramafic rocks and related chromite ores of the Main Ophiolite Belt of the Urals. *Geol. Ore Depos.* **2009**, *51*, 162–178. [[CrossRef](#)]
47. Badanina, I.Y.; Malitch, K.N.; Murzin, V.V.; Khiller, V.V.; Glavatskiy, S.P. Mineralogical and geochemical particularities of PGE mineralization of the Verkh-Neivinsk dunite-harzburgite massif (Middle Urals, Russia). *Proc. Inst. Geol. Geochem. UB RAS* **2013**, *160*, 188–192. (In Russian)
48. Murzin, V.V.; Sustavov, S.G. New data about minerals of laurite-erlichmanite series and their As-bearing varieties. *Dokl. Akad. Nauk* **2000**, *370*, 380–382. (In Russian)
49. Badanina, I.Y.; Malitch, K.N.; Belousova, E.A.; Murzin, V.V.; Lord, R.A. Osmium isotope systematics of Ru–Os–Ir alloys and Ru–Os sulfides of the dunite–harzburgite massifs: A synthesis of new data. *Proc. Inst. Geol. Geochem. UB RAS* **2014**, *161*, 167–172. (In Russian)
50. Malitch, K.N.; Badanina, I.Y.; Belousova, E.A.; Murzin, V.V. Chemical and Os-isotopic composition of Ru-Os sulfides from Verkh-Neivinsky dunite-harzburgite massif (Middle Urals, Russia). *Dokl. Earth Sci.* **2018**, *483*, 1437–1441. [[CrossRef](#)]
51. Murzin, V.V.; Badanina, I.Y.; Malitch, K.N.; Ignatiev, A.V.; Velivetskaya, T.A. Sulfur isotope composition of Ru-Os sulfides from the Verkh-Neivinsky dunite-harzburgite massif (Middle Urals, Russia): New data. *Dokl. Earth Sci.* **2019**, *488*, 1097–1099. [[CrossRef](#)]
52. Riesberg, L.; Lorand, J.P. Longevity of subcontinental mantle lithosphere from osmium isotope systematics in orogenic peridotite massifs. *Nature* **1995**, *376*, 159–162. [[CrossRef](#)]
53. Malitch, K.N. *Platinum-Group Elements in Clinopyroxenite-Dunite Massifs of the Eastern Siberia (Geochemistry, Mineralogy, and Genesis)*; St. Petersburg Cartographic Factory VSEGEI Press: St. Petersburg, Russia, 1999; p. 296. (In Russian)
54. Malitch, K.N.; Kostoyanov, A.I. Model Re-Os isotopic age of the PGE mineralization at the Gulinsk Massif (at the northern Siberian Platform, Russia). *Geol. Ore Depos.* **1999**, *41*, 126–135.
55. Walker, R.J.; Prichard, H.M.; Ishiwatari, A.; Pimentel, M. The osmium isotopic composition of convecting upper mantle deduced from ophiolite chromites. *Geochim. Cosmochim. Acta* **2002**, *66*, 329–345. [[CrossRef](#)]
56. Malitch, K.N. Osmium isotope constraints on contrasting sources and prolonged melting in the Proterozoic upper mantle: Evidence from ophiolitic Ru-Os sulfides and Ru-Os-Ir alloys. *Chem. Geol.* **2004**, *208*, 157–173. [[CrossRef](#)]
57. Carlson, R.W. Application of the Pt–Re–Os isotopic systems to mantle geochemistry and geochronology. *Lithos* **2005**, *82*, 249–272. [[CrossRef](#)]
58. Walker, R.J.; Brandon, A.D.; Bird, J.M.; Piccoli, P.M.; McDonough, W.F.; Ash, R.D. ¹⁸⁷Os–¹⁸⁶Os systematics of Os-Ir-Ry alloy grains from southwestern Oregon. *Earth Planet. Sci. Lett.* **2005**, *230*, 211–236. [[CrossRef](#)]
59. Tessalina, S.G.; Bourdon, B.; Gannoun, A.; Campas, F.; Birck, J.-L.; Allegre, C.J. Complex proterozoic to paleozoic history of the upper mantle recorded in the Urals lherzolite massifs by Re–Os and Sm–Nd systematics. *Chem. Geol.* **2007**, *240*, 61–84. [[CrossRef](#)]
60. Coggon, J.A.; Nowell, G.M.; Pearson, D.G.; Parman, S.W. Application of the ¹⁹⁰Pt–¹⁸⁶Os isotope system to dating platinum mineralization and ophiolite formation: An example from the Meratus Mountains, Borneo. *Econ. Geol.* **2011**, *106*, 93–117. [[CrossRef](#)]
61. González-Jiménez, J.M.; Gervilla, F.; Griffin, W.L.; Proenza, J.A.; Augé, T.; O'Reilly, S.Y.; Pearson, N.J. Os-isotope variability within sulfides from podiform chromitites. *Chem. Geol.* **2012**, *291*, 224–235. [[CrossRef](#)]
62. Tessalina, S.G.; Malitch, K.N.; Augé, T.; Puchkov, V.N.; Belousova, E.; McInnes, B. Origin of the Nizhny Tagil clinopyroxenite-dunite massif (Uralian Platinum Belt, Russia): Insights from PGE and Os isotope systematics. *J. Petrol.* **2005**, *56*, 2297–2318. [[CrossRef](#)]
63. Malitch, K.N.; Anikina, E.V.; Badanina, I.Y.; Belousova, E.A.; Pushkarev, E.V.; Khiller, V.V. Chemical composition and osmium isotope systematics of primary and secondary platinum-group mineral assemblages from high-Mg chromite of the Nurali lherzolite massif, South Urals, Russia. *Geol. Ore Depos.* **2016**, *58*, 1–19. [[CrossRef](#)]
64. Malitch, K.N.; Belousova, E.A.; Griffin, W.L.; Badanina, I.Y.; Knauf, V.V.; O'Reilly, S.Y.; Pearson, N.J. Laurite and zircon from the Finero chromitites (Italy): New insights into evolution of the subcontinental mantle. *Ore Geol. Rev.* **2017**, *90*, 210–225. [[CrossRef](#)]
65. Lugué, A.; Nowell, G.M.; Pushkarev, E.; Ballhaus, C.; Wirth, R.; Schreiber, A.; Gottman, I. ¹⁹⁰Pt–¹⁸⁶Os geochronometer reveals open system behaviour of ¹⁹⁰Pt–⁴He isotope system. *Geochem. Perspect. Lett.* **2019**, *11*, 44–48. [[CrossRef](#)]

66. Malitch, K.N.; Puchtel, I.S.; Belousova, E.A.; Badanina, I.Y. Contrasting platinum-group mineral assemblages of the Kondyor massif (Russia): Implications for the sources of HSE in zoned-type ultramafic massifs. *Lithos* **2020**, *376–377*, 105800. [[CrossRef](#)]
67. Pearson, N.J.; Alard, O.; Griffin, W.L.; Jackson, S.E.; O'Reilly, S.Y. In situ measurement of Re-Os isotopes in mantle sulfides by laser ablation multicollector-inductively coupled plasma mass spectrometry: Analytical methods and preliminary results. *Geochim. Cosmochim. Acta* **2002**, *66*, 1037–1050. [[CrossRef](#)]
68. Lorand, J.-P.; Alard, O. Platinum-group element abundances in the upper mantle: New constraints from in situ and whole-rock analyses of Massif Central xenoliths (France). *Geochim. Cosmochim. Acta* **2001**, *65*, 2789–2806. [[CrossRef](#)]
69. Malitch, K.N.; Lopatin, G.G. New data on the metallogeny of the unique Guli clinopyroxenite-dunite Massif, Northern Siberia, Russia. *Geol. Ore Depos.* **1997**, *39*, 209–218.
70. Merkle, R.K.W.; Malitch, K.N.; Grasser, P.P.H.; Badanina, I.Y. Native osmium from the Guli Massif, Northern Siberia (Russia). *Mineral. Petrol.* **2012**, *104*, 115–127. [[CrossRef](#)]
71. Shirey, S.B.; Walker, R.J. The Re-Os isotope system in cosmochemistry and high-temperature geochemistry. *Annu. Rev. Earth Planet. Sci.* **1998**, *26*, 423–500. [[CrossRef](#)]
72. Walker, R.J.; Carlson, R.W.; Shirey, S.B.; Boyd, F.R. Os, Sr, Nd, and Pb isotope systematics of Southern African peridotite xenoliths: Implications for the chemical evolution of subcontinental mantle. *Geochim. Cosmochim. Acta* **1989**, *53*, 1583–1595. [[CrossRef](#)]
73. Smoliar, M.I.; Walker, R.J.; Morgan, J.W. Re-Os ages of group IIA, IIIA, IVA, and IVB meteorites. *Science* **1996**, *271*, 1099–1102. [[CrossRef](#)]
74. Walker, R.J.; Horan, M.F.; Morgan, J.W.; Becker, H.; Grossman, J.N.; Rubin, A.E. Comparative ¹⁸⁷Re-¹⁸⁷Os systematics of chondrites: Implications regarding early solar system processes. *Geochim. Cosmochim. Acta* **2002**, *66*, 4187–4201. [[CrossRef](#)]
75. Yin, Q.; Jagoutz, E.; Palme, H.; Wanke, H. NUR—A possible proxy for CHUR reference for Re-Os system derived from ¹⁸⁷Os/¹⁸⁸Os ratio of the Allende CAI. In Proceedings of the Lunar and Planetary Science Conference XXVII, Houston, TX, USA, 18–22 March 1996; pp. 1475–1476.
76. Meisel, T.; Walker, R.J.; Irving, A.J.; Lorand, J.-P. Osmium isotopic composition of mantle xenoliths: A global perspective. *Geochim. Cosmochim. Acta* **2001**, *65*, 1311–1323. [[CrossRef](#)]
77. Ignatiev, A.V.; Velivetskaya, T.A.; Budnitskiy, S.Y.; Yakovenko, V.V.; Vysotskiy, S.V.; Levitskii, V.I. Precision analysis of multisulfur isotopes in sulfides by femtosecond laser ablation GC-IRMS at high spatial resolution. *Chem. Geol.* **2018**, *493*, 316–326. [[CrossRef](#)]
78. Velivetskaya, T.A.; Ignatiev, A.V.; Yakovenko, V.V.; Vysotskiy, S.V. An improved femtosecond laser-ablation fluorination method for measurements of sulfur isotopic anomalies ($\Delta^{33}\text{S}$ and $\Delta^{36}\text{S}$) in sulfides with high precision. *Rapid Commun. Mass Spectrom.* **2019**, *33*, 1722–1729. [[CrossRef](#)] [[PubMed](#)]
79. Harris, D.C.; Cabri, L.J. Nomenclature of platinum-group-element alloys: Review and revision. *Can. Mineral.* **1991**, *29*, 231–237.
80. Boyd, F.R.; Mertzman, S.A. Composition and structure of the Kaapvaal lithosphere, southern Africa. In *Magmatic Processes: Physicochemical Principles*; Mysen, B.O., Ed.; Geochemical Society: Washington, WA, USA, 1987; Volume 1, pp. 13–24.
81. Gaul, O.F.; Griffin, W.L.; O'Reilly, S.Y.; Pearson, D.G. Mapping olivine compositions in the lithospheric mantle. *Earth Planet. Sci. Lett.* **2000**, *182*, 223–235. [[CrossRef](#)]
82. Pearson, D.G.; Canil, D.; Shirey, S.B. Mantle samples included in volcanic rocks: Xenoliths and diamonds. In *Treatise on Geochemistry*, 2nd ed.; Holland, H.D., Turekian, K.K., Eds.; Elsevier: Amsterdam, The Netherlands, 2014; Volume 3, pp. 169–253.
83. Badanina, I.Y.; Malitch, K.N.; Murzin, V.V.; Proskurnin, V.F. Geochemical particularities of PGE and gold in chromitites of dunite-harzburgite and clinopyroxenite-dunite massifs. *Proc. Inst. Geol. Geochem. Uzb Ras* **2019**, *166*, 95–101. (In Russian)
84. Melcher, F.; Grum, W.; Simon, G.; Thalhammer, T.V.; Stumpfl, E.F. Petrogenesis of the ophiolitic giant chromite deposits of Kempirsai, Kazakhstan: A study of solid and fluid inclusions in chromite. *J. Petrol.* **1997**, *38*, 1419–1458. [[CrossRef](#)]
85. Bird, J.M.; Bassett, W.A. Evidence of a deep mantle history in terrestrial osmium-iridium-ruthenium alloys. *J. Geophys. Res.* **1980**, *85*, 5461–5470. [[CrossRef](#)]
86. Cabri, L.J.; Harris, D.C. Zoning in Os-Ir alloys and the relation of the geological and tectonic environment of the source rocks to the bulk Pt:Pt+Ir+Os ratio for placers. *Can. Mineral.* **1975**, *13*, 266–274.
87. Peck, D.C.; Keays, R.R.; Ford, R.J. Direct crystallization of refractory platinum-group element alloys from boninitic magmas: Evidence from western Tasmania. *Aust. J. Earth Sci.* **1992**, *39*, 373–387. [[CrossRef](#)]
88. Bird, J.M.; Meibom, A.; Frei, R.; Nagler, T.F. Osmium and lead isotopes of rare OsIrRu minerals: Derivation from the core-mantle boundary region? *Earth Planet. Sci. Lett.* **1999**, *170*, 83–92. [[CrossRef](#)]
89. Thode, H.G.; Monster, J.; Dunford, H.B. Sulphur isotope geochemistry. *Geochim. Cosmochim. Acta* **1961**, *25*, 159–174. [[CrossRef](#)]
90. Gao, X.; Thiemens, M.H. Isotopic composition and concentration of sulfur in carbonaceous chondrites. *Geochim. Cosmochim. Acta* **1993**, *57*, 3159–3169. [[CrossRef](#)]
91. Gao, X.; Thiemens, M.H. Variations in the isotopic composition of sulfur in enstatite and ordinary chondrites. *Geochim. Cosmochim. Acta* **1993**, *57*, 3171–3176. [[CrossRef](#)]
92. Pushkarev, Y.D. Two types of interaction of crustal and mantle matter and a new approach to the problems of deep ore formation. *Dokl. Russ. Acad. Sci.* **1997**, *335*, 524–526. (In Russian)
93. Ripley, E.M.; Li, C. Applications of stable and radiogenic isotopes to magmatic Cu-Ni-PGE deposits: Examples and cautions. *Earth Sci. Front.* **2007**, *14*, 124–132. [[CrossRef](#)]
94. Meibom, A.; Frei, R.; Sleep, N.H. Osmium isotopic compositions of Os-rich platinum group element alloys from the Klamath and Siskiyou Mountains. *J. Geophys. Res.* **2004**, *109*, B02203. [[CrossRef](#)]

95. Brandon, A.D.; Walker, R.J.; Puchtel, I.S. Platinum-osmium isotope evolution of the Earth's mantle: Constraints from chondrites and Os-rich alloys. *Geochim. Cosmochim. Acta* **2006**, *70*, 2093–2103. [[CrossRef](#)]
96. Lazarenkov, V.G.; Landa, E.A. Evidences for non-intrusive nature of the Kondyor massif and problems of the mantle diapirism. *Proc. Russ. Acad. Sci. Geol. Ser.* **1992**, *6*, 102–113. (In Russian)
97. Burg, J.P.; Bodinier, J.-L.; Gerya, N.; Bedini, R.-M.; Boudier, F.; Dautria, J.-M.; Prikhodko, V.; Efimov, A.; Pupier, E.; Balanec, J.-L. Translithospheric mantle diapirism: Geological evidence and numerical modeling of the Kondyor zoned ultramafic complex (Russian Far-East). *J. Petrol.* **2009**, *50*, 289–321. [[CrossRef](#)]
98. Edwards, R.; Wasserburg, G.J. The age and emplacement of obducted oceanic crust in the Urals from Sm–Nd and Rb–Sr systematics. *Earth Planet. Sci. Lett.* **1985**, *72*, 389–404. [[CrossRef](#)]
99. Melcher, F.; Grum, W.; Thalhammer, T.V.; Thalhammer, O.A.R. The giant chromite deposits at Kempirsai, Urals: Constraints from trace element (PGE, REE) and isotope data. *Miner. Depos.* **1999**, *34*, 250–272. [[CrossRef](#)]
100. Krasnobaev, A.A.; Valizer, P.M. Zircons and zircon geochronology of gabbro from the Nurali massif (Southern Urals). *Lithosphere* **2018**, *18*, 574–584. (In Russian) [[CrossRef](#)]
101. Krasnobaev, A.A.; Rusin, A.I.; Busharina, S.V.; Rodionov, N.V. Zirconology of ultramafic rocks from the Vostochnotagilskii massif (Middle Urals). *Dokl. Earth Sci.* **2014**, *455*, 441–445. [[CrossRef](#)]
102. Parkinson, I.J.; Hawkesworth, C.J.; Cohen, A.S. Ancient mantle in a modern arc: Osmium isotopes in Izu-Bonin-Mariana forearc peridotites. *Science* **1998**, *281*, 2011–2013. [[CrossRef](#)]
103. Snow, J.E.; Schmidt, G. Proterozoic melting in the northern peridotite massif, Zabargad island: Os isotopic evidence. *Terra Nova* **1999**, *11*, 45–50. [[CrossRef](#)]
104. Spetsius, Z.V.; Belousova, E.A.; Griffin, W.L.; O'Reilly, S.Y.; Pearson, N.J. Archean sulfide inclusions in Paleozoic zircon megacrysts from the Mir kimberlite, Yakutia: Implications for the dating of diamonds. *Earth Planet. Sci. Lett.* **2002**, *199*, 111–126. [[CrossRef](#)]
105. Dobretsov, N.L.; Kirdyashkin, A.G. *Deep-Level Geodynamics*; Swets and Zeitlinger: Rotterdam, The Netherlands, 1998; 328p.
106. Savelieva, G.N.; Suslov, P.V.; Larionov, A.N. Vendian tectono-magmatic events in mantle ophiolitic complexes of the Polar Urals: U–Pb dating of zircon from chromitite. *Geotectonics* **2007**, *41*, 105–113. [[CrossRef](#)]
107. Fershtater, G.B. *Paleozoic Intrusive Magmatism of the Middle and Southern Urals*; Ural Branch of RAS: Ekaterinburg, Russia, 2013; 368p. (In Russian)
108. Krasnobaev, A.A.; Anfilogov, V.N. Zircons: Implications for dunite genesis. *Dokl. Earth Sci.* **2014**, *456*, 535–538. [[CrossRef](#)]
109. Krasnobaev, A.A.; Valizer, P.M.; Anfilogov, V.N.; Sergeev, S.A.; Rusin, A.I.; Busharina, S.V.; Medvedeva, E.V. Zirconology of ultrabasic rocks of the Karabash massif (Southern Urals). *Dokl. Earth Sci.* **2016**, *469*, 674–679. [[CrossRef](#)]